

Unit-level mixed effects models for conditional extremes

KOKI MOMOKI^{1*}and TAKUMA YOSHIDA²

^{1,2}*Graduate School of Science and Engineering, Kagoshima University
1-21-40 Korimoto, Kagoshima, Kagoshima, 890-8580, Japan*

Abstract

Extreme value theory (EVT) provides an elegant mathematical tool for statistically analyzing rare events. When data are collected from multiple population subgroups, the scientific interest of researchers would generally be to improve the estimates obtained directly from each subgroup because some subgroups may have less data available for extreme value analysis. To achieve this, we incorporate the mixed effects model (MEM) into the regression technique in EVT. In small area estimation, the MEM has attracted considerable attention as a primary tool for providing reliable estimates for subgroups with small sample sizes, that is, “small area.” The key idea of the MEM is to incorporate information from all subgroups into a single model and to borrow strength from other subgroups to improve estimates by subgroup. Using this property, the MEM may contribute to reducing the bias and variance of the direct estimates for each subgroup, which result from the asymptotic specification of EVT. This prompts us to evaluate MEM’s effectiveness in EVT through theoretical studies and numerical experiments, including its application to assessing the risk of heavy rainfall in Japan.

Extreme value index regression; Extreme value theory; Mixed effects model; Pareto-type distribution; Risk assessment; Unit-level data

1 Introduction

Statistical analysis of rare events is crucial for risk assessment in various fields, including meteorology, environment, seismology, finance, economics, and insurance. Extreme value theory (EVT) provides an elegant mathematical method for assessing these rare events.

In the framework of univariate EVT, the generalized extreme value distribution (Fisher and Tippett 1928; Gumbel 1958) and generalized Pareto distribution (GPD, Davison and Smith 1990) are standard models for fitting extreme value data. In

*E-mail: k3499390@kadai.jp

addition, the class of GPDs with unbounded tails is called the Pareto-type distribution, which has been recognized as an important model for analyzing heavy-tailed data (Beirlant et al. 2004). As an important direction of developmental works on EVT, these models have been extended to regression models to incorporate covariate information into extreme value analysis (Davison and Smith 1990; Beirlant and Goegebeur 2003; Beirlant et al. 2004; Wang and Tsai 2009). However, few regression techniques have been developed for unit-level data in extreme value analysis.

The data category of interest is denoted by $\{(Y_{ij}, \mathbf{X}_{ij}), i = 1, 2, \dots, n_j, j = 1, 2, \dots, J\}$, where J is the number of population subgroups, n_j is the sample size from the j th population subgroup, Y_{ij} is the response of interest, and \mathbf{X}_{ij} is the vector of relevant covariates. In the literature on small area estimation (SAE), such data are referred to as unit-level data and each population subgroup is then called an “area” (Rao and Molina 2015; Sugashawa and Kubokawa 2020; Molina et al. 2022). In particular, the area with a small sample size is the so-called “small area,” which is described in detail by Jiang (2017). Examples of areas include a geographic region such as a state, county, or municipality, or a demographic group such as a specific age-sex-race group. From the definition on p. 173 of Rao and Molina (2015), unit-level data implies that the number of areas J is known, and each observation is explicitly allocated to one of the areas.

Our purpose is not to pool data from multiple areas into a single area by clustering, nor to create a new set of areas with heterogeneous characteristics (see Bottolo et al. 2003, Rohrbeck and Tawn 2021, de Carvalho et al. 2023, Dupuis et al. 2023, and references therein). Contrary to these approaches, our objective is to develop an advanced risk assessment model that utilizes information from all areas simultaneously, instead of constructing models by area. However, if information from all areas is modeled as parameters, the number of parameters depends on J . Therefore, when J is large, the fully parametric model can lead to a large bias in the parameter estimates (Section 4 of Ruppert et al. 2003; Broström and Holmberg 2011). Thus, we aim to construct an EVT model for unit-level data, which does not require many parameters. For this purpose, we incorporate the unit-level mixed effects model into EVT. Among the different types of mixed effects models, the unit-level mixed effects model refers to the mixed effects model for the unit-level data mentioned above. In the following, we will simply refer to this as the mixed effects model (MEM). The MEM has been described in Jiang (2007), Wu (2009), Jiang (2017), and the references therein. This model can provide reliable estimates for each area by capturing the heterogeneity between areas as a latent structure rather than parameters. In SAE (Torabi 2019; Sugashawa and Kubokawa 2020), the efficiency of the MEM is well known for its so-called “borrowing of strength” property (Dempster et al. 1981). Dempster et al. (1981) described the “borrowing of strength” as follows:

Using concepts of variability between and within units, one can improve estimates based on the data from a single unit by the appropriate use of data from the remaining units. (p. 341)

In other words, the “borrowing of strength” shows us that the direct estimates based only on area-specific data are improved by leveraging information from other areas (Section 1 of Diallo and Rao 2018). For the small areas mentioned above, the “borrowing of strength” would be particularly helpful because the accuracy of

their direct estimates is not sufficiently guaranteed (Molina and Rao 2010; Diallo and Rao 2018). In extreme value analysis, we use only data with small or large values; hence, the effective sample size tends to be small for some areas. Thus, the MEM is crucial for obtaining more efficient estimators for extreme value analysis. However, to the best of our knowledge, there are no results for integrating the MEM and EVT. Therefore, it would be important to demonstrate that the “borrowing of strength” is also valid for extreme value analysis. The purpose of this study is to reveal such considerations theoretically and numerically.

In this study, we incorporate the MEM into the extreme value index (EVI) included in the Pareto-type distribution. For this model, we first pick the extreme value data for each area by peak over threshold. Subsequently, the parameters included in the EVI model are estimated by the maximum likelihood estimation method. The random components called random effects in the MEM, which express the latent area-wise differences in the parameters, are predicted by the conditional mode. We investigate the asymptotic normality of the proposed estimator (see, Section 3.2). From this asymptotic normality, we find that the variance of the proposed estimator improves as the number of areas J increases. In other words, the proposed estimator is generally stable, even when the effective sample sizes are small for certain areas. Owing to this property, the proposed estimator can reduce the severe bias of Pareto-type modeling by setting reasonably higher thresholds while achieving stable behavior. Furthermore, we show numerically through the Monte Carlo simulation study that our estimates for each area, obtained by combining the proposed estimator and predictor, not only have significantly smaller variances than the direct estimates but are also less biased (see, Section 4.3). Surprisingly, for EVT, the “borrowing of strength” of the MEM contributes to reducing both bias and variance.

As an application, we analyze heavy rainfall in various locations (areas) in Japan. Certainly, the risk of heavy rainfall varies by the location where meteorological observations are recorded, and an accurate assessment of this risk is highly desirable. For several locations, the effective sample size with high precipitation is extremely small (see, Section 5.3.2). However, we expect that the “borrowing of strength” of the MEM will improve the performance of the predicted EVI for such locations. Along with some analyses, we will demonstrate the effectiveness of the proposed MEM for assessing the risk of heavy rainfall in Japan. We note that considering multiple locations aligns with the mathematical condition where the number of areas J is large. Our asymptotic theory of the estimator, as previously mentioned, is established under $J \rightarrow \infty$.

The remainder of this article is organized as follows. Section 2 proposes the regression model using the MEM for the Pareto-type distribution. Section 3 investigates its asymptotic properties. Section 4 examines the finite sample performance of our model. As an application, Section 5 analyzes a real dataset of heavy rainfall in Japan using the proposed method. Section 6 summarizes this study and discusses future research. The technical details are described in the Appendix.

2 Model and method

Define \mathbb{R}^+ as the set of all positive real numbers. Throughout this article, we consider the unit-level data

$$\{(Y_{ij}, \mathbf{X}_{ij}) \in \mathbb{R}^+ \times \mathbb{R}^p, i = 1, 2, \dots, n_j, j = 1, 2, \dots, J\}, \quad (1)$$

where J is the number of areas, n_j is the sample size of the j th area, Y_{ij} is the continuous random variable corresponding to the response of interest, and \mathbf{X}_{ij} is the random vector representing associated predictors. Here, $(Y_{ij}, \mathbf{X}_{ij})$ is regarded as the observation for the i th unit in the j th area. We denote the index sets by $\mathcal{J} := \{1, 2, \dots, J\}$ and $\mathcal{N}_j := \{1, 2, \dots, n_j\}$. In the following Sections 2.1-2.4, we describe the proposed MEM and associated estimation and prediction methods.

2.1 Mixed effects model under Pareto-type distribution

Let $\mathbf{X}_{ij}, i \in \mathcal{N}_j, j \in \mathcal{J}$ be an independent and identically distributed (i.i.d.) random sample from the same distribution. Subsequently, we assume that for each $i \in \mathcal{N}_j$ and $j \in \mathcal{J}$, the response Y_{ij} is conditionally independently obtained from certain conditional distribution $F_j(y | \mathbf{x}) = P(Y_{ij} \leq y | \mathbf{X}_{ij} = \mathbf{x})$ for the given \mathbf{X}_{ij} , where F_j is determined for each $j \in \mathcal{J}$. In this study, we are interested in the right tail behavior of each F_j . Here, the right tail of each F_j is modeled by the Pareto-type distribution as

$$F_j(y | \mathbf{x}) = 1 - y^{-1/\gamma_j(\mathbf{x})} \mathcal{L}_j(y; \mathbf{x}), \quad j \in \mathcal{J}, \quad (2)$$

where $\gamma_j(\mathbf{x}) > 0$ is an EVI function, and $\mathcal{L}_j(y; \mathbf{x})$ is a conditional slowly varying function with respect to y given \mathbf{x} , i.e., for any \mathbf{x} and $s > 0$, $\mathcal{L}_j(ys; \mathbf{x})/\mathcal{L}_j(y; \mathbf{x}) \rightarrow 1$ as $y \rightarrow \infty$. The EVI function $\gamma_j(\mathbf{x})$, which determines the heaviness of the right tail of F_j , is assumed to be the classical linear model formulated as follows:

$$\gamma_j(\mathbf{x}) = \exp \left\{ (\boldsymbol{\theta}_{jA}^0)^\top \mathbf{x}_A + (\boldsymbol{\theta}_B^0)^\top \mathbf{x}_B \right\}, \quad j \in \mathcal{J}, \quad (3)$$

where $\mathbf{x} := (\mathbf{x}_A^\top, \mathbf{x}_B^\top)^\top \in \mathbb{R}^{p_A} \times \mathbb{R}^{p_B}$, and $\boldsymbol{\theta}_{jA}^0 \in \mathbb{R}^{p_A}$ and $\boldsymbol{\theta}_B^0 \in \mathbb{R}^{p_B}$ are regression coefficient vectors. $\boldsymbol{\theta}_{jA}^0$ is different for each area, whereas $\boldsymbol{\theta}_B^0$ is common to all areas. The partitioning of covariates $\mathbf{X}_{ij} := (\mathbf{X}_{Aij}^\top, \mathbf{X}_{Bij}^\top)^\top \in \mathbb{R}^{p_A} \times \mathbb{R}^{p_B}$ is then organized by user specification or model selection (see, Section 5.3.1). When $J = 1$, the above model is reduced to that of Wang and Tsai (2009). The purpose of the model (2) with (3) is to estimate the parameter vectors $\boldsymbol{\theta}_{1A}^0, \boldsymbol{\theta}_{2A}^0, \dots, \boldsymbol{\theta}_{JA}^0$ and $\boldsymbol{\theta}_B^0$. However, this model has $(J \times p_A + p_B)$ parameters; hence, if J is large, the associated estimators may be severely biased (Section 4 of Ruppert et al. 2003; Broström and Holmberg 2011). To overcome this bias problem, we use the MEM rather than the fully parametric model (2) with (3).

For $p_A \leq p$, we introduce the random effects $\mathbf{U}_j \in \mathbb{R}^{p_A}, j \in \mathcal{J}$ such that

$$\mathbf{U}_1, \mathbf{U}_2, \dots, \mathbf{U}_J \stackrel{\text{i.i.d.}}{\sim} N(\mathbf{0}, \boldsymbol{\Sigma}_0), \quad (4)$$

where $N(\mathbf{0}, \boldsymbol{\Sigma}_0)$ refers to the multivariate normal distribution with zero mean vector and unknown covariance matrix $\boldsymbol{\Sigma}_0$. The MEM uses these random effects to express

the differences in F_j between areas as a latent structure. Let $F(y | \mathbf{u}_j, \mathbf{x}) := P(Y_{ij} \leq y | \mathbf{U}_j = \mathbf{u}_j, \mathbf{X}_{ij} = \mathbf{x})$ be the conditional distribution function of Y_{ij} given $\mathbf{U}_j = \mathbf{u}_j$ and $\mathbf{X}_{ij} = \mathbf{x}$. In this expression, the information regarding the differences in F_j between areas is assigned to F by \mathbf{u}_j . Note that the random effects \mathbf{U}_j , $j \in \mathcal{J}$ are not observed as data.

As an alternative model to (2) with (3), the Pareto-type distribution with the MEM is defined as follows:

$$F(y | \mathbf{u}_j, \mathbf{x}) = 1 - y^{-1/\gamma(\mathbf{u}_j, \mathbf{x})} \mathcal{L}(y; \mathbf{u}_j, \mathbf{x}), \quad j \in \mathcal{J}, \quad (5)$$

where $\mathcal{L}(y; \mathbf{u}_j, \mathbf{x})$ conditional on $\mathbf{U}_j = \mathbf{u}_j$ and $\mathbf{X}_{ij} = \mathbf{x}$ is a slowly varying function with respect to y . Accordingly, as an extension of (3) to the MEM, the EVI function $\gamma(\mathbf{u}_j, \mathbf{x})$ is assumed to be

$$\gamma(\mathbf{u}_j, \mathbf{x}) = \exp \left\{ (\boldsymbol{\theta}_A^0 + \mathbf{u}_j)^\top \mathbf{x}_A + (\boldsymbol{\theta}_B^0)^\top \mathbf{x}_B \right\}, \quad j \in \mathcal{J}. \quad (6)$$

Compared to (3), the area-wise differences in the slope of log-EVI with respect to \mathbf{X}_{Aij} are represented by \mathbf{u}_j , $j \in \mathcal{J}$ as a latent structure. Thus, the total number of parameters in the model (5) with (6) is $p + p_A(p_A + 1)/2$, which is independent of J and less than that of the fully parametric model (2) with (3) when J is large. Here, $p_A(p_A + 1)/2$ is the number of parameters included in $\boldsymbol{\Sigma}_0$.

The simplest model of (6) is the location-shifting MEM with $p_A = 1$ and $\mathbf{X}_{Aij} \equiv 1$, denoted $\boldsymbol{\theta}_A^0$ and \mathbf{u}_j by scalars θ_A^0 and u_j ,

$$\gamma(u_j, \mathbf{x}_B) = \exp \left\{ \theta_A^0 + u_j + (\boldsymbol{\theta}_B^0)^\top \mathbf{x}_B \right\}, \quad j \in \mathcal{J}, \quad (7)$$

which can be regarded as an EVI regression version of the nested error regression model (Battese et al. 1988). The model (7) indicates that the intercept of $\log \gamma$ accepts the heterogeneity between areas, although any covariate has the common slope of $\log \gamma$ across all areas. The nested error regression model is useful for SAE (Diallo and Rao 2018; Sugiyama and Kubokawa 2020). In fact, our application in Section 5 confirms that (7) is the most effective compared to other setups of \mathbf{X}_{Aij} and \mathbf{X}_{Bij} . Alternatively, the case $p = p_A$ yields the most complicated model of (6), indicating that the slope of $\log \gamma$ with respect to each covariate varies across areas.

2.2 Approximate maximum likelihood estimator

In this section, we construct the estimators of the unknown parameters $\{\boldsymbol{\theta}_A^0, \boldsymbol{\theta}_B^0, \boldsymbol{\Sigma}_0\}$ included in the model (5) with (6).

Let $F_{\omega_j}(y | \mathbf{u}_j, \mathbf{x}) := P(Y_{ij} \leq y | \mathbf{U}_j = \mathbf{u}_j, \mathbf{X}_{ij} = \mathbf{x}, Y_{ij} > \omega_j)$ be the conditional distribution function given $\mathbf{U}_j = \mathbf{u}_j$, $\mathbf{X}_{ij} = \mathbf{x}$ and $Y_{ij} > \omega_j$, where $\omega_j \in \mathbb{R}^+$, $j \in \mathcal{J}$ are thresholds. If ω_j is sufficiently high, we have

$$F_{\omega_j}(y | \mathbf{u}_j, \mathbf{x}) \approx 1 - \left(\frac{y}{\omega_j} \right)^{-1/\gamma(\mathbf{u}_j, \mathbf{x})}, \quad j \in \mathcal{J}. \quad (8)$$

Using (8) instead of (5), we can remove \mathcal{L} for the estimation of γ . The density of Y_{ij} given $\mathbf{U}_j = \mathbf{u}_j$, $\mathbf{X}_{ij} = \mathbf{x}$ and $Y_{ij} > \omega_j$ is obtained as follows:

$$f_{w_j}(y | \mathbf{u}_j, \mathbf{x}) \approx \omega_j^{-1} \gamma(\mathbf{u}_j, \mathbf{x})^{-1} \left(\frac{y}{\omega_j} \right)^{-1/\gamma(\mathbf{u}_j, \mathbf{x})-1}, \quad j \in \mathcal{J}. \quad (9)$$

The estimation using data exceeding thresholds is the so-called peak-over-threshold method (Hill 1975; Wang and Tsai 2009).

We assume that \mathbf{U}_j and \mathbf{X}_{ij} , for $i \in \mathcal{N}_j$ and $j \in \mathcal{J}$, are independent. Furthermore, we assume that Y_{ij} given \mathbf{U}_j and \mathbf{X}_{ij} is conditionally independent for $i \in \mathcal{N}_j$ and $j \in \mathcal{J}$ and has the distribution function (5) (Jiang et al. 2022). Using (9), we then define the likelihood of $(\boldsymbol{\theta}_A^0, \boldsymbol{\theta}_B^0, \boldsymbol{\Sigma}_0)$ as

$$L(\boldsymbol{\theta}_A, \boldsymbol{\theta}_B, \boldsymbol{\Sigma}) := \prod_{j=1}^J E_{\mathbf{U}_j} \left[\prod_{i \in \mathcal{N}_j: Y_{ij} > \omega_j} f_{\omega_j}(Y_{ij} | \mathbf{U}_j, \mathbf{X}_{ij}) \right],$$

where $E_{\mathbf{U}_j}$ denotes the expectation over the random effects distribution, $(\boldsymbol{\theta}_A^\top, \boldsymbol{\theta}_B^\top)^\top \in \mathbb{R}^{p_A} \times \mathbb{R}^{p_B}$ is any vector corresponding to $((\boldsymbol{\theta}_A^0)^\top, (\boldsymbol{\theta}_B^0)^\top)^\top$, and $\boldsymbol{\Sigma} \in \mathbb{R}^{p_A \times p_A}$ is any positive definite matrix corresponding to $\boldsymbol{\Sigma}_0$. The above L is derived from the standard definition of the likelihood for the MEM because \mathbf{U}_j , $j \in \mathcal{J}$ are unobserved random variables, unlike the data (1) (Section 2 of Wu 2009). Accordingly, the log-likelihood of $(\boldsymbol{\theta}_A^0, \boldsymbol{\theta}_B^0, \boldsymbol{\Sigma}_0)$ can be expressed as

$$\begin{aligned} \ell(\boldsymbol{\theta}_A, \boldsymbol{\theta}_B, \boldsymbol{\Sigma}) &:= \log L(\boldsymbol{\theta}_A, \boldsymbol{\theta}_B, \boldsymbol{\Sigma}) \\ &\approx \sum_{j=1}^J \log \int_{\mathbb{R}^{p_A}} \phi(\mathbf{u}; \mathbf{0}, \boldsymbol{\Sigma}) \exp \left\{ \sum_{i=1}^{n_j} \left[-(\boldsymbol{\theta}_A + \mathbf{u})^\top \mathbf{X}_{Aij} - \boldsymbol{\theta}_B^\top \mathbf{X}_{Bij} \right. \right. \\ &\quad \left. \left. - \exp \left\{ -(\boldsymbol{\theta}_A + \mathbf{u})^\top \mathbf{X}_{Aij} - \boldsymbol{\theta}_B^\top \mathbf{X}_{Bij} \right\} \log \frac{Y_{ij}}{\omega_j} \right] I(Y_{ij} > \omega_j) \right\} d\mathbf{u} + C, \end{aligned} \quad (10)$$

where $I(\cdot)$ is an indicator function that returns 1 if $Y_{ij} > \omega_j$ and 0 otherwise, $\phi(\cdot; \mathbf{0}, \boldsymbol{\Sigma})$ is a density function of $N(\mathbf{0}, \boldsymbol{\Sigma})$, and C is a suitable constant independent of $(\boldsymbol{\theta}_A, \boldsymbol{\theta}_B, \boldsymbol{\Sigma})$. Again, because \mathbf{U}_j , $j \in \mathcal{J}$ are not observed as data, the log-likelihood (10) includes the integral over the domain \mathbb{R}^{p_A} of the random effects. We denote the approximated maximum likelihood estimator of $(\boldsymbol{\theta}_A^0, \boldsymbol{\theta}_B^0, \boldsymbol{\Sigma}_0)$ by $(\hat{\boldsymbol{\theta}}_A, \hat{\boldsymbol{\theta}}_B, \hat{\boldsymbol{\Sigma}})$, which is the maximizer of the right-hand side of (10).

2.3 Prediction of random effects

In the proposed model (5) with (6), we are not only interested in estimating the parameters $\{\boldsymbol{\theta}_A^0, \boldsymbol{\theta}_B^0, \boldsymbol{\Sigma}_0\}$, but also in predicting the random effects \mathbf{U}_j , $j \in \mathcal{J}$. Here, we propose the conditional mode method to predict the random effects \mathbf{U}_j , $j \in \mathcal{J}$ (Santner and Duffy 1989; Section 11 of Wu 2009). Now, the conditional density function of $(\mathbf{U}_1, \mathbf{U}_2, \dots, \mathbf{U}_J)$ given the data (1) is proportional to

$$\prod_{j=1}^J \left\{ \phi(\mathbf{u}_j; \mathbf{0}, \boldsymbol{\Sigma}_0) \prod_{i \in \mathcal{N}_j: Y_{ij} > \omega_j} f_{\omega_j}(Y_{ij} | \mathbf{u}_j, \mathbf{X}_{ij}) \right\},$$

as a function of $(\mathbf{u}_1, \mathbf{u}_2, \dots, \mathbf{u}_J)$. Then, the predictor of \mathbf{U}_j is defined as the mode of this conditional distribution by

$$\tilde{\mathbf{u}}_j := \operatorname{argmax}_{\mathbf{u}_j \in \mathbb{R}^{p_A}} \phi(\mathbf{u}_j; \mathbf{0}, \boldsymbol{\Sigma}_0) \prod_{i \in \mathcal{N}_j: Y_{ij} > \omega_j} f_{\omega_j}(Y_{ij} | \mathbf{u}_j, \mathbf{X}_{ij}), \quad j \in \mathcal{J}, \quad (11)$$

where f_{ω_j} and $(\boldsymbol{\theta}_A^0, \boldsymbol{\theta}_B^0, \boldsymbol{\Sigma}_0)$ included in f_{ω_j} are replaced by (9) and the estimator $(\hat{\boldsymbol{\theta}}_A, \hat{\boldsymbol{\theta}}_B, \hat{\boldsymbol{\Sigma}})$, respectively.

2.4 Threshold selection

The thresholds ω_j , $j \in \mathcal{J}$ in (10) are tuning parameters that balance between the quality of the approximation (9) and the amount of data exceeding the thresholds. By setting higher thresholds, we can generally improve the estimation bias but the estimator becomes more unstable. Conversely, if we lower the thresholds, the estimator behaves more stably, but may be more biased. Therefore, these thresholds ω_j , $j \in \mathcal{J}$ should be selected appropriately, considering this trade-off relationship. Here, for each area, we apply the discrepancy measure (Wang and Tsai 2009), which considers the goodness of fit of the model, to select the area-wise optimal threshold. In the simulation studies in Section 4, we verify the performance of the proposed estimator using this threshold selection method.

3 Asymptotic properties

We investigate the asymptotic properties of the proposed estimator $(\hat{\boldsymbol{\theta}}_A, \hat{\boldsymbol{\theta}}_B, \hat{\boldsymbol{\Sigma}})$. In general, the following three types of asymptotic scenarios may be considered:

- (i) J remains finite while n_j , $j \in \mathcal{J}$ tend to infinity.
- (ii) n_j , $j \in \mathcal{J}$ remain finite while J tends to infinity.
- (iii) J and n_j , $j \in \mathcal{J}$ tend to infinity.

In applications using the peak-over-threshold method, the sample size of the threshold exceedances is often small (see, Section 5.3.2). Therefore, we must use as many related area sources as possible to improve the estimates for each area. Such a scenario can be expressed mathematically as $J \rightarrow \infty$. Therefore, (i) does not match the background of using the MEM for extreme value analysis. Meanwhile, if the thresholds ω_j , $j \in \mathcal{J}$ as well as the sample sizes exceeding the thresholds are fixed, the consistency of the proposed estimator would not be shown because the bias occurring from the approximation (9) cannot be improved. Ignoring such a bias is outside the concept of EVT (Theorems 2 and 4 of Wang and Tsai 2009). This implies that (ii) is also not realistic in our study. To evaluate the impact of the choice of the thresholds and bias of the proposed estimator, we must consider the case where $\omega_j \rightarrow \infty$, $j \in \mathcal{J}$ and the sample sizes exceeding the thresholds also tend to infinity, which can be taken under $n_j \rightarrow \infty$, $j \in \mathcal{J}$. Consequently, (iii) is most important for establishing EVT for the MEM, and we assume this case in the following Sections 3.1 and 3.2.

Nie (2007) and Jiang et al. (2022) referred to the asymptotic normality of the maximum likelihood estimator of the generalized mixed effects model under (iii). Thus, we can say that the following Theorem 1 extends their results from the generalized mixed effects model to the MEM for EVT.

3.1 Conditions

Let $n_{j0} := \sum_{i=1}^{n_j} I(Y_{ij} > \omega_j)$, which is the sample size exceeding the threshold ω_j for the j th area. Additionally, we define $n_0 := J^{-1} \sum_{j=1}^J n_{j0}$ as the average of the effective sample sizes of all areas. Note that n_{j0} , $j \in \mathcal{J}$ and n_0 are random variables, not constants. For the case (iii) defined earlier, we assume that for any $j \in \mathcal{J}$, the threshold ω_j diverges to infinity in tandem with the sequence of J and the j th within-area sample size n_j . Accordingly, we denote ω_j by $\omega_{(J,n_j)}$. The asymptotic properties of the proposed estimator rely on the following assumptions (A1)-(A6):

(A1) $\mathcal{L}(y; \mathbf{u}, \mathbf{x})$ in (5) belongs to the Hall class (Hall 1982), that is,

$$\mathcal{L}(y; \mathbf{u}, \mathbf{x}) = c_0(\mathbf{u}, \mathbf{x}) + c_1(\mathbf{u}, \mathbf{x})y^{-\beta(\mathbf{u}, \mathbf{x})} + \epsilon(y; \mathbf{u}, \mathbf{x}), \quad (12)$$

where $c_0(\mathbf{u}, \mathbf{x}) > 0$, $c_1(\mathbf{u}, \mathbf{x})$, $\beta(\mathbf{u}, \mathbf{x}) > 0$ and $\epsilon(y; \mathbf{u}, \mathbf{x})$ are continuous and bounded. Furthermore, $\epsilon(y; \mathbf{u}, \mathbf{x})$ satisfies

$$\sup_{\mathbf{u} \in \mathbb{R}^{p_A}, \mathbf{x} \in \mathbb{R}^p} \left\{ y^{\beta(\mathbf{u}, \mathbf{x})} \epsilon(y; \mathbf{u}, \mathbf{x}) \right\} \rightarrow 0 \quad \text{as } y \rightarrow \infty.$$

(A2) There exists a bounded and continuous function $\delta : \mathbb{R}^{p_A} \times \mathbb{R}^p \rightarrow \mathbb{R}^+$ such that

$$\sup_{\mathbf{u} \in \mathbb{R}^{p_A}, \mathbf{x} \in \mathbb{R}^p} \left| \frac{P(Y_{ij} > y \mid \mathbf{U}_j = \mathbf{u}, \mathbf{X}_{ij} = \mathbf{x})}{P(Y_{ij} > y \mid \mathbf{U}_j = \mathbf{u})} - \delta(\mathbf{u}, \mathbf{x}) \right| \rightarrow 0 \quad \text{as } y \rightarrow \infty.$$

(A3) As $n_j \rightarrow \infty$, $j \in \mathcal{J}$ and $J \rightarrow \infty$,

$$\inf_{j \in \mathcal{J}, \mathbf{u} \in \mathbb{R}^{p_A}} n_j P(Y_{ij} > \omega_{(J,n_j)} \mid \mathbf{U}_j = \mathbf{u}) \rightarrow \infty.$$

(A4) There exist some bounded and continuous functions $d_j : \mathbb{R}^{p_A} \rightarrow \mathbb{R}^+$, $j \in \mathcal{J}$ such that under given $\mathbf{U}_j = \mathbf{u}$, $n_{j0}/n_0 \rightarrow^P d_j(\mathbf{u})$ uniformly for all $j \in \mathcal{J}$ and $\mathbf{u} \in \mathbb{R}^{p_A}$ as $n_j \rightarrow \infty$, $j \in \mathcal{J}$ and $J \rightarrow \infty$, where the symbol “ \rightarrow^P ” represents convergence in probability.

(A5) $n_0/J \rightarrow^P 0$ as $n_j \rightarrow \infty$, $j \in \mathcal{J}$ and $J \rightarrow \infty$.

(A6) There exist some bounded and continuous functions $\mathbf{b}_{Kj} : \mathbb{R}^{p_A} \rightarrow \mathbb{R}$ for $j \in \mathcal{J}$ and $K \in \{A, B\}$ such that

$$\sup_{j \in \mathcal{J}, \mathbf{u} \in \mathbb{R}^{p_A}} \left\| \frac{J^{1/2} n_0^{1/2} E_{\mathbf{X}_{ij}} [\mathbf{X}_{Kij} \zeta_j(\mathbf{u}, \mathbf{X}_{ij})]}{P(Y_{ij} > \omega_{(J,n_j)} \mid \mathbf{U}_j = \mathbf{u})^{1/2}} - \mathbf{b}_{Kj}(\mathbf{u}) \right\| \rightarrow 0$$

as $n_j \rightarrow \infty$, $j \in \mathcal{J}$ and $J \rightarrow \infty$, where

$$\zeta_j(\mathbf{u}, \mathbf{x}) := \frac{c_1(\mathbf{u}, \mathbf{x}) \gamma(\mathbf{u}, \mathbf{x}) \beta(\mathbf{u}, \mathbf{x})}{1 + \gamma(\mathbf{u}, \mathbf{x}) \beta(\mathbf{u}, \mathbf{x})} \omega_{(J,n_j)}^{-1/\gamma(\mathbf{u}, \mathbf{x}) - \beta(\mathbf{u}, \mathbf{x})}$$

and $\|\cdot\|$ refers to the Euclidean norm.

(A1) and (A2) regularize the tail behavior of the conditional response distribution F in (5) (Wang and Tsai 2009; Ma et al. 2019). (A3)-(A6) impose the constraints on the divergence rates of the thresholds $\omega_{(J,n_j)}$, $j \in \mathcal{J}$. (A3) implies that for

each $j \in \mathcal{J}$, the effective sample size n_{j0} asymptotically diverges to infinity. Under (A4), n_{j0} , $j \in \mathcal{J}$ are not critically different from each other. Furthermore, (A5) implies that the number of areas J is relatively larger than the effective sample sizes n_{j0} , $j \in \mathcal{J}$. (A5) is needed to express mathematically the relationship between the divergence rates of J and $\omega_{(J, n_j)}$. (A6) is related to the asymptotic bias of the proposed estimator. If (A6) fails, the consistency of the proposed estimator may not be guaranteed.

3.2 Asymptotic normality

Let \mathbf{M} be a matrix of zeros and ones such that $\mathbf{M}\text{vech}(\mathbf{A}) = \text{vec}(\mathbf{A})$ for all symmetric matrices $\mathbf{A} \in \mathbb{R}^{p_A \times p_A}$, where $\text{vec}(\cdot)$ is a vector operator, and $\text{vech}(\cdot)$ is a vector half operator that stacks the lower triangular half of the given $d \times d$ square matrix into the single vector of length $d(d+1)/2$ (Magnus and Neudecker 1988). The Moore-Penrose inverse of \mathbf{M} is $\mathbf{M}_* := (\mathbf{M}^\top \mathbf{M})^{-1} \mathbf{M}^\top$.

For the maximum likelihood estimator $(\hat{\theta}_A, \hat{\theta}_B, \hat{\Sigma})$, we obtain the following result.

Theorem 1. *Suppose that (A1)-(A6) hold. Then, as $n_j \rightarrow \infty$, $j \in \mathcal{J}$ and $J \rightarrow \infty$,*

$$\begin{bmatrix} J^{1/2}(\hat{\theta}_A - \theta_A^0) \\ J^{1/2}n_0^{1/2}(\hat{\theta}_B - \theta_B^0) \\ J^{1/2}\text{vech}(\hat{\Sigma} - \Sigma_0) \end{bmatrix} + \begin{bmatrix} n_0^{-1/2}\mathbf{b}_A \\ \mathbf{b}_B \\ n_0^{-1/2}\mathbf{b}_C \end{bmatrix} \xrightarrow{D} N\left(\mathbf{0}, \begin{bmatrix} \Delta_A & \mathbf{O} & \mathbf{O} \\ \mathbf{O} & \Delta_B & \mathbf{O} \\ \mathbf{O} & \mathbf{O} & \Delta_C \end{bmatrix}\right),$$

where the symbol “ \xrightarrow{D} ” denotes convergence in the distribution, \mathbf{O} s are zero matrices of appropriate size, and \mathbf{b}_K and Δ_K , $K \in \{A, B, C\}$ are defined as follows:

$$\begin{aligned} \mathbf{b}_A &:= \lim_{J \rightarrow \infty} J^{-1} \sum_{j=1}^J E \left[d_j(\mathbf{U}_j)^{-1/2} \Phi_{AA}(\mathbf{U}_j)^{-1} \mathbf{b}_{Aj}(\mathbf{U}_j) \right], \\ \mathbf{b}_B &:= \lim_{J \rightarrow \infty} J^{-1} \sum_{j=1}^J \Delta_B E \left[d_j(\mathbf{U}_j)^{1/2} \left\{ \mathbf{b}_{Bj}(\mathbf{U}_j) - \Phi_{AB}(\mathbf{U}_j)^\top \Phi_{AA}(\mathbf{U}_j)^{-1} \mathbf{b}_{Aj}(\mathbf{U}_j) \right\} \right], \\ \mathbf{b}_C &:= \lim_{J \rightarrow \infty} J^{-1} \sum_{j=1}^J \Delta_C \mathbf{M}_* (\Sigma_0 \otimes \Sigma_0)^{-1} \\ &\quad \times \text{vec} \left(E \left[d_j(\mathbf{U}_j)^{-1/2} \left\{ \mathbf{U}_j \mathbf{b}_{Aj}(\mathbf{U}_j)^\top \Phi_{AA}(\mathbf{U}_j)^{-1} + \Phi_{AA}(\mathbf{U}_j)^{-1} \mathbf{b}_{Aj}(\mathbf{U}_j) \mathbf{U}_j^\top \right\} \right] \right), \\ \Delta_A &:= \Sigma_0, \\ \Delta_B &:= E \left[\Phi_{BB}(\mathbf{U}_j) - \Phi_{AB}(\mathbf{U}_j)^\top \Phi_{AA}(\mathbf{U}_j)^{-1} \Phi_{AB}(\mathbf{U}_j) \right]^{-1} \quad \text{and} \\ \Delta_C &:= 2 \left\{ \mathbf{M}_* (\Sigma_0 \otimes \Sigma_0)^{-1} \mathbf{M}_*^\top \right\}^{-1}, \end{aligned}$$

where $\Phi_{K_1 K_2}(\mathbf{U}_j) := E_{\mathbf{X}_{ij}}[\delta(\mathbf{U}_j, \mathbf{X}_{ij}) \mathbf{X}_{K_1 ij} \mathbf{X}_{K_2 ij}^\top]$ for $K_1, K_2 \in \{A, B\}$, and \otimes is the Kronecker product.

Remark 1. From Theorem 1, $\hat{\boldsymbol{\theta}}_A$ and $\hat{\boldsymbol{\Sigma}}$ are \sqrt{J} -consistent, and $\hat{\boldsymbol{\theta}}_B$ is $\sqrt{Jn_0}$ -consistent. Furthermore, $\hat{\boldsymbol{\theta}}_A$, $\hat{\boldsymbol{\theta}}_B$ and $\hat{\boldsymbol{\Sigma}}$ are asymptotically independent. If J and n_j , $j \in \mathcal{J}$ are sufficiently large, the covariance matrix of the proposed estimator is obtained as

$$\text{cov} \left[\hat{\boldsymbol{\theta}}_A \right] \approx J^{-1} \boldsymbol{\Delta}_A, \quad \text{cov} \left[\hat{\boldsymbol{\theta}}_B \right] \approx (Jn_0)^{-1} \boldsymbol{\Delta}_B \quad \text{and} \quad \text{cov} \left[\text{vech} \left(\hat{\boldsymbol{\Sigma}} \right) \right] \approx J^{-1} \boldsymbol{\Delta}_C. \quad (13)$$

Theorem 1 also reveals the asymptotic bias of the proposed estimator induced by the approximation (9). If J and n_j , $j \in \mathcal{J}$ are sufficiently large, it can be approximated as

$$\begin{aligned} E \left[\hat{\boldsymbol{\theta}}_A \right] - \boldsymbol{\theta}_A^0 &\approx (Jn_0)^{-1/2} \mathbf{b}_A, \\ E \left[\hat{\boldsymbol{\theta}}_B \right] - \boldsymbol{\theta}_B^0 &\approx (Jn_0)^{-1/2} \mathbf{b}_B \quad \text{and} \\ E \left[\text{vech} \left(\hat{\boldsymbol{\Sigma}} \right) \right] - \text{vech} \left(\boldsymbol{\Sigma}_0 \right) &\approx (Jn_0)^{-1/2} \mathbf{b}_C. \end{aligned}$$

As in (A6), \mathbf{b}_{Kj} depends on the EVI function $\gamma(\mathbf{u}, \mathbf{x})$, and the proposed estimator is more biased for larger $\gamma(\mathbf{u}, \mathbf{x})$, that is, the heavier the right tail of the response distribution. Furthermore, \mathbf{b}_{Kj} is also affected by $\beta(\mathbf{u}, \mathbf{x})$ defined in (12), and the proposed estimator is more biased for smaller $\beta(\mathbf{u}, \mathbf{x})$. Meanwhile, $c_0(\mathbf{u}, \mathbf{x})$ in (12), which is the scaling constant to ensure that the upper bound of (5) is equal to one, is not related to the asymptotic bias of the proposed estimator.

Remark 2. From Theorem 1, we can confirm the good compatibility between the MEM and EVT as follows. In extreme value analysis, we want to set the threshold as high as possible to ensure a good fit with the Pareto distribution, as illustrated in (9). However, the estimator may have a large variance because the amount of available data is small. Meanwhile, the variance of the proposed estimator for (5) with (6) depends strongly on the number of areas J and improves as J increases, as shown in (13). Note that the magnitude of J is unaffected by the choice of thresholds ω_j , $j \in \mathcal{J}$, unlike n_0 . Therefore, even if some thresholds are high, the proposed estimator is expected to remain stable as long as J is sufficiently large. Note that estimating the bias of the proposed estimator is a difficult problem because $\beta(\mathbf{u}, \mathbf{x})$ and $c_1(\mathbf{u}, \mathbf{x})$ in (12) must be estimated. However, if J is sufficiently large, by setting reasonably high thresholds, we may avoid this bias estimation problem while ensuring the stability of the estimator. Such phenomena are confirmed numerically in Section 4 below.

Remark 3. Theorem 1 is directly applicable to confidence interval construction and statistical hypothesis testing on the parameters $\boldsymbol{\theta}_A^0$, $\boldsymbol{\theta}_B^0$ and $\boldsymbol{\Sigma}_0$. To obtain more efficient estimates, the choice of covariates is crucial. Alternatively, including exceedingly many meaningless covariates in the model will adversely affect the parameter estimations, and the “borrowing of strength” will not be effective. Therefore, we must verify the efficiency of the selected explanatory variables. Hypothesis testing is useful for this purpose. The typical statement of such a hypothesis test is whether each component of $\boldsymbol{\theta}_A^0$ and $\boldsymbol{\theta}_B^0$ is significantly different from zero or not. If we aim

to organize this test, we must estimate Δ_B^{-1} , which can be naturally estimated by

$$\hat{\Delta}_B^{-1} := J^{-1} \sum_{j=1}^J \left(\hat{\Phi}_{BBj} - \hat{\Phi}_{ABj}^\top \hat{\Phi}_{AAj}^{-1} \hat{\Phi}_{ABj} \right), \quad (14)$$

where $\hat{\Phi}_{K_1 K_2 j} := n_{j0}^{-1} \sum_{i=1}^{n_j} \mathbf{X}_{K_1 ij} \mathbf{X}_{K_2 ij}^\top I(Y_{ij} > \omega_j)$, $K_1, K_2 \in \{A, B\}$. In Section 5.3.2, the hypothesis test on θ_B^0 is demonstrated for a real dataset.

As described in Section 2.1, an important example of (6) is the type of the nested error regression model (7). For the model (7), Theorem 1 can be simplified to the following Corollary 1. Let $\sigma_0^2 := \text{var}[U_j]$ and denote its proposed estimator as $\hat{\sigma}^2$.

Corollary 1. *Suppose that (A1)-(A6) hold. Then, as $n_j \rightarrow \infty$, $j \in \mathcal{J}$ and $J \rightarrow \infty$,*

$$\begin{bmatrix} J^{1/2} (\hat{\theta}_A - \theta_A^0) \\ J^{1/2} n_0^{1/2} (\hat{\theta}_B - \theta_B^0) \\ J^{1/2} (\hat{\sigma}^2 - \sigma_0^2) \end{bmatrix} + \begin{bmatrix} n_0^{-1/2} v_A \\ \mathbf{v}_B \\ n_0^{-1/2} v_C \end{bmatrix} \xrightarrow{D} N \left(\mathbf{0}, \begin{bmatrix} \sigma_0^2 & \mathbf{O} & \mathbf{O} \\ \mathbf{O} & \Omega_B & \mathbf{O} \\ \mathbf{O} & \mathbf{O} & 2(\sigma_0^2)^2 \end{bmatrix} \right),$$

where v_A , \mathbf{v}_B , v_C and Ω_B are defined as follows:

$$\begin{aligned} v_A &:= \lim_{J \rightarrow \infty} J^{-1} \sum_{j=1}^J E \left[d_j(U_j)^{-1/2} v_{Aj}(U_j) \right], \\ \mathbf{v}_B &:= \lim_{J \rightarrow \infty} J^{-1} \sum_{j=1}^J \Omega_B E \left[d_j(U_j)^{1/2} \{ \mathbf{b}_{Bj}(\mathbf{U}_j) - v_{Aj}(U_j) \mathbf{\Psi}_B(U_j) \} \right], \\ v_C &:= \lim_{J \rightarrow \infty} J^{-1} \sum_{j=1}^J 4 \text{vec} \left(E \left[d_j(U_j)^{-1/2} v_{Aj}(U_j) U_j \right] \right) \quad \text{and} \\ \Omega_B &:= E \left[\mathbf{\Phi}_{BB}(U_j) - \mathbf{\Psi}_B(U_j) \mathbf{\Psi}_B(U_j)^\top \right]^{-1}, \end{aligned}$$

where $v_{Aj}(U_j)$ is $\mathbf{b}_{Aj}(U_j)$ with $p_A = 1$ and $\mathbf{X}_{Aij} \equiv 1$, $\mathbf{\Psi}_B(U_j) := E_{\mathbf{X}_{Bij}} [\delta(U_j, \mathbf{X}_{Bij}) \mathbf{X}_{Bij}]$, and $\mathbf{\Phi}_{BB}(U_j)$ is defined in Theorem 1.

4 Simulation

From (8) and (9), we can approximate the distribution of $\log(Y_{ij}/\omega_j)$ conditional on \mathbf{U}_j , \mathbf{X}_{ij} and $Y_{ij} > \omega_j$ by the exponential distribution, which belongs to the gamma distribution (Wang and Tsai 2009). Therefore, our estimator and predictor can be easily implemented using the function `glmer()` with `family=Gamma(link="log")` in the package `lme4` (Bates et al. 2015) within the R computing environment (R Core Team 2021). In this function, when $p_A = 1$, the integral over the random effects space in the log-likelihood (10) is approximated by the adaptive Gauss-Hermite quadrature, and $\hat{\Sigma}$ and $(\hat{\theta}_A, \hat{\theta}_B)$ are optimized by “bobyqa” and “Nelder Mead”, respectively.

In the following Sections 4.1-4.3, we investigate the performance of our method through some simulation studies that use the above package.

4.1 Practicality for asymptotic normality of the estimator

We explain the procedure for simulating the dataset $\{(Y_{ij}, \mathbf{X}_{ij})\}_{i \in \mathcal{N}_j, j \in \mathcal{J}}$. Let denote $\mathbf{X}_{ij} = (X_{ij}^{(1)}, X_{ij}^{(2)})^\top \in \mathbb{R}^2$ and set $X_{ij}^{(1)} \equiv 1$. First, we generate $\{X_{ij}^{(2)}\}_{i \in \mathcal{N}_j, j \in \mathcal{J}}$ from the standard normal distribution or uniform distribution on $[-\sqrt{3}, \sqrt{3}]$. Thus, in both cases, $X_{ij}^{(2)}$ has zero mean and unit variance. The next step obtains U_1, U_2, \dots, U_J from $N(0, \sigma^2)$ with $\sigma^2 = 0.2$. Finally, for each $i \in \mathcal{N}_j$ and $j \in \mathcal{J}$, we generate Y_{ij} using a given conditional response distribution $F(\cdot | U_j, X_{ij}^{(2)})$. The above procedure is also used in the next section.

In this section, we provide a simulation study to illustrate the applicability of Corollary 1 on finite samples. This is positioned as a preliminary study for hypothesis testing in the real data example in Section 5.3.2. Here, we use the Pareto distribution

$$F(y | U_j, X_{ij}^{(2)}) = 1 - y^{-1/\gamma(U_j, X_{ij}^{(2)})} \quad (15)$$

and apply the nested error regression type model (7) with $\mathbf{X}_{Aij} = X_{ij}^{(1)}$ and $\mathbf{X}_{Bij} = X_{ij}^{(2)}$ as

$$\gamma(U_j, X_{ij}^{(2)}) = \exp\left(\theta_A^{(1)} + U_j + \theta_B^{(2)} X_{ij}^{(2)}\right), \quad (16)$$

where $(\theta_A^{(1)}, \theta_B^{(2)}) = (-0.5, 0.2)$. Let us denote the proposed estimator of $(\theta_A^{(1)}, \theta_B^{(2)}, \sigma^2)$ by $(\hat{\theta}_A^{(1)}, \hat{\theta}_B^{(2)}, \hat{\sigma}^2)$. Because the Pareto distribution (15) satisfies (12) with $\beta(U_j, X_{ij}^{(2)}) = \infty$, this estimator does not have the asymptotic bias. Thus, we do not use the thresholds ω_j , $j \in \mathcal{J}$, that is, the effective sample size n_{j0} for each area is unchanged from n_j .

Under the above model setups, from Corollary 1, the standardized estimators $J^{1/2}(\hat{\theta}_A^{(1)} - \theta_A^{(1)})/\sigma$, $(Jn_0)^{1/2}(\hat{\theta}_B^{(2)} - \theta_B^{(2)})$ and $J^{1/2}(\hat{\sigma}^2 - \sigma^2)/(\sqrt{2}\sigma^2)$ are asymptotically distributed as $N(0, 1)$. We obtain $\boldsymbol{\Omega}_B = 1$ under this simulation setting. To obtain the empirical distributions of these standardized estimators, we use 500 sets of datasets and repeatedly estimate the parameters $\{\theta_A^{(1)}, \theta_B^{(2)}, \sigma^2\}$ from each of the datasets. Figures 1 and 2 show the Q-Q plots for the obtained standardized estimates against $N(0, 1)$ for the normal covariate and uniform covariate, respectively. In these figures, (J, n_{j0}) varies by column as $(20, 10)$, $(40, 10)$, $(10, 20)$, $(20, 20)$, $(40, 20)$, $(80, 20)$, $(80, 40)$, and $(150, 100)$. Furthermore, the bands in each panel are the 95% pointwise confidence bands created by the function `geom_qq_band()` with `bandType="boot"` in the package `qqplotr` (Almeida et al. 2018) within the R. If all generated $\{U_j\}_{j \in \mathcal{J}}$ are close to each other, σ^2 may be estimated to be zero by `glmer()`. Thus, for $J = 10$ and $J = 20$, the Q-Q plot for σ^2 contained several equal values. Comparing Figures 1 and 2, the type of the distribution of $X_{ij}^{(2)}$ did not significantly affect the results. In addition, from Figures 1 and 2, we can see that the empirical distributions of the standardized estimators of $\theta_A^{(1)}$ and σ^2 had heavier tails than $N(0, 1)$, but this tendency disappeared with increasing J and n_{j0} . In contrast to $\theta_A^{(1)}$ and σ^2 , the Q-Q plot for $\theta_B^{(2)}$ was good for all pairs of (J, n_{j0}) . Therefore, these results reflect the claims of Corollary 1. Meanwhile, the closest setting to the application in Section 5 is the case $(J, n_{j0}) = (150, 100)$. From Figures 1

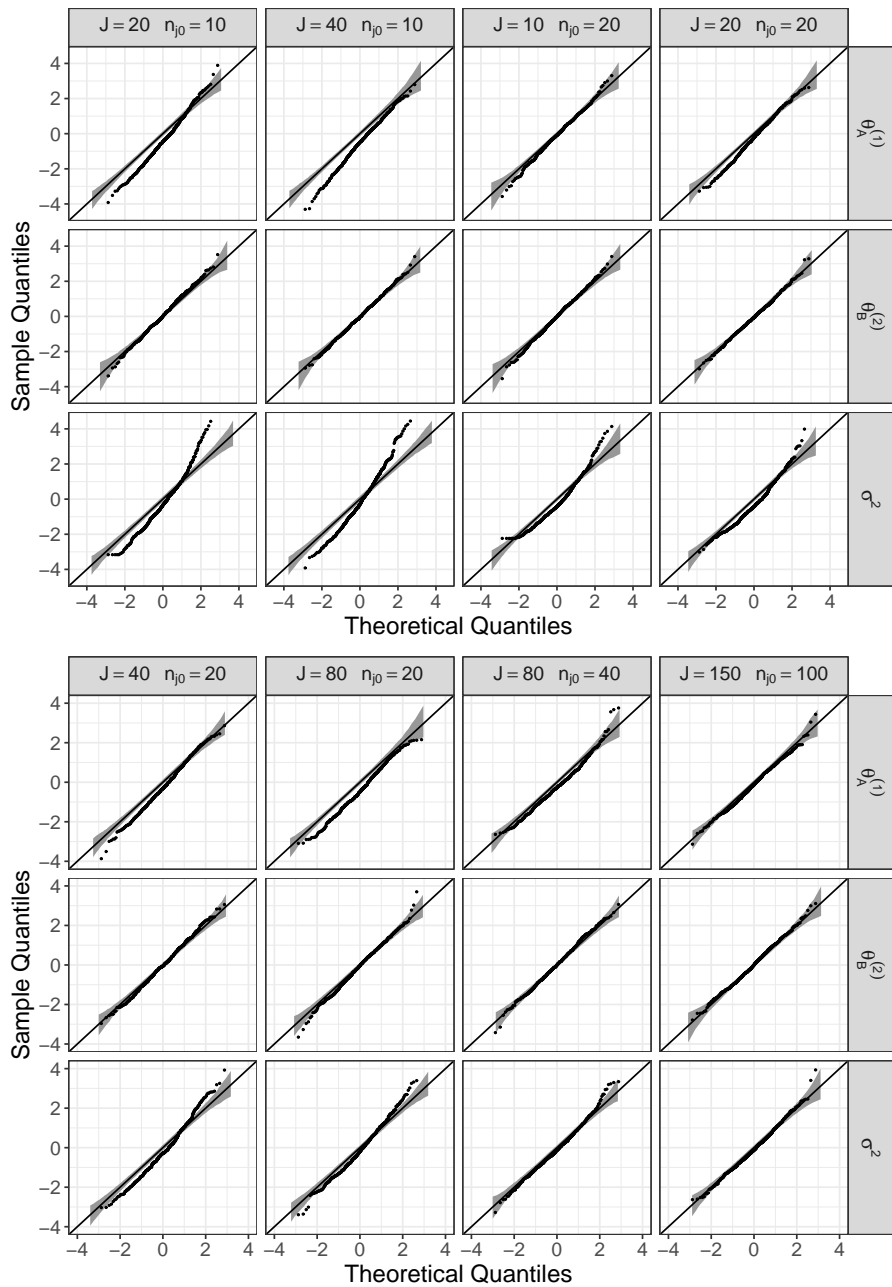


Figure 1: Results of the simulation with the normal covariate: Q-Q plot for the standardized estimates against $N(0, 1)$

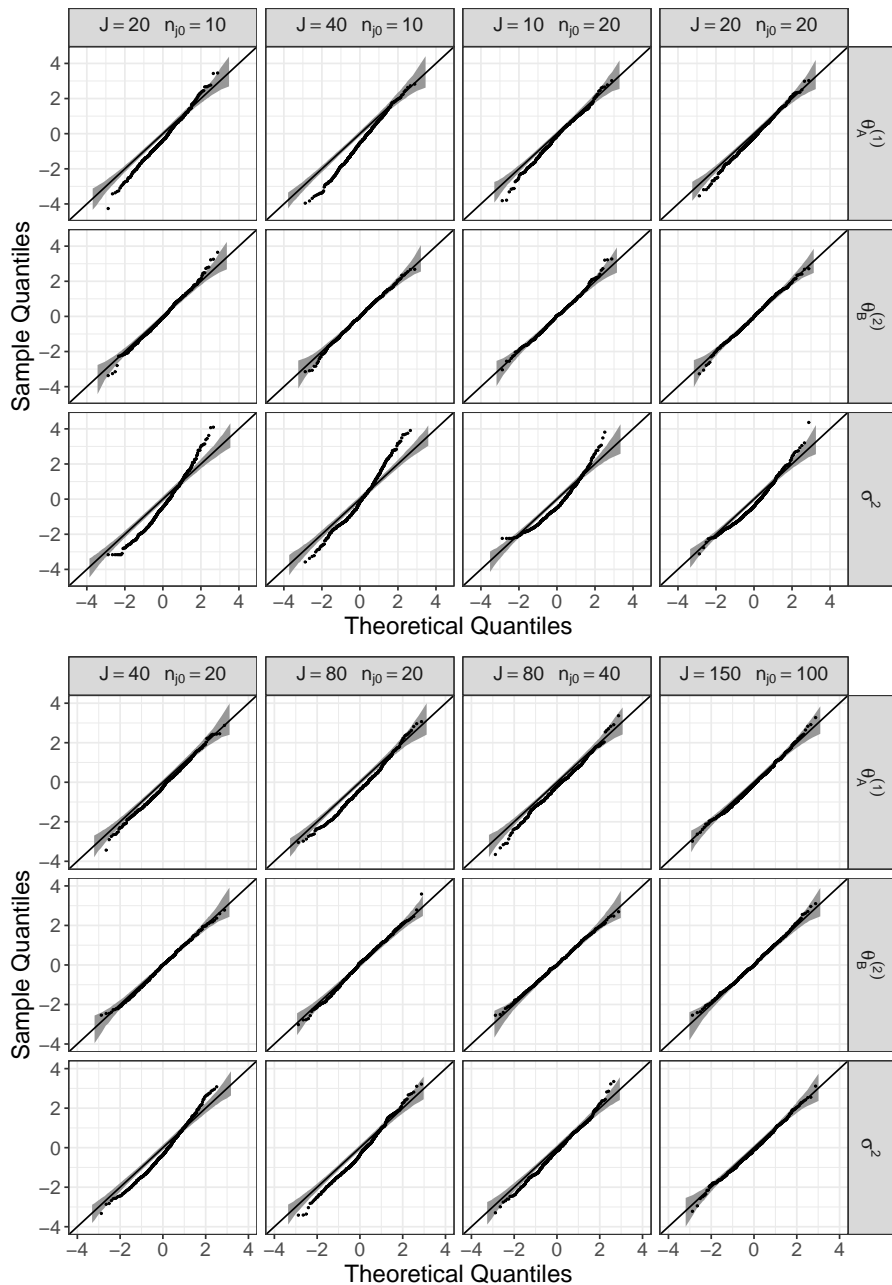


Figure 2: Results of the simulation with the uniform covariate: Q-Q plot for the standardized estimates against $N(0, 1)$

and 2, our Corollary 1 with $(J, n_{j0}) = (150, 100)$ adequately captured the behavior of our estimator.

4.2 Behavior of the estimator for numerous areas

Typically, when J is large, the fully parametric model such as (2) with (3) results in a large bias. As described in Section 4.3, its variance is slightly improved compared to analyzing the areas separately, whereas its bias is rather larger. Therefore, we are interested in the numerical performance of the proposed MEM for large J .

To obtain the dataset according to the procedure in Section 4.1, we use (16) and the conditional distribution (a) or (b):

(a) Student's t -distribution

$$F(y | U_j, X_{ij}^{(2)}) = \int_{-\infty}^y \frac{\Gamma((\nu(U_j, X_{ij}^{(2)}) + 1)/2)}{\sqrt{\nu(U_j, X_{ij}^{(2)})} \pi \Gamma(\nu(U_j, X_{ij}^{(2)})/2)} \\ \times \left\{ 1 + \frac{t^2}{\nu(U_j, X_{ij}^{(2)})} \right\}^{-\{\nu(U_j, X_{ij}^{(2)})+1\}/2} dt$$

with $\nu(U_j, X_{ij}^{(2)}) := \gamma(U_j, X_{ij}^{(2)})^{-1}$, where $\Gamma(\cdot)$ is a gamma function. This distribution belongs to the Pareto-type distribution with $\beta(U_j, X_{ij}^{(2)}) \equiv 2$ in (12).

(b) Burr distribution

$$F(y | U_j, X_{ij}^{(2)}) = 1 - \left\{ \frac{\eta}{\eta + y^{\tau(U_j, X_{ij}^{(2)})}} \right\}^\kappa$$

with $\eta = 1$, $\kappa = 1$ and $\tau(U_j, X_{ij}^{(2)}) := \gamma(U_j, X_{ij}^{(2)})^{-1}$. This distribution satisfies (12) with $\beta(U_j, X_{ij}^{(2)}) = \tau(U_j, X_{ij}^{(2)})$.

For (a), we directly implement the t -distribution for a given non-integer degree of freedom. As described in Remark 1 of Section 3.2, the proposed estimator is more biased for smaller $\beta(U_j, X_{ij}^{(2)})$.

In advance, we generate the unit-level data with 500 areas and $n_j = 1000$ using the above procedure. Subsequently, we use a part of the dataset according to the following rules. The number of areas J is increased by a factor of 10 from 50 to 500. Furthermore, in the discrepancy measure in Section 2.4, we use the top 10 to T th responses in the j th area as the candidates for the j th threshold ω_j , where T varies from 20 to 200 in increments of 20. Roughly, a smaller T means that higher thresholds ω_j , $j \in \mathcal{J}$ are chosen. For each J and T , we obtain the estimator $(\hat{\theta}_A^{(1)}, \hat{\theta}_B^{(2)}, \hat{\sigma}^2)$. Here, we iterate the estimation for 100 sets of unit-level data. Figures 3-6 show the sample squared bias and variance of the estimator for each J and T . The details are given in the description of each figure. Overall, we can see that our estimator remained stable if J was sufficiently large, even if T was small. Based on the first row of each figure, our estimator then did not suffer from a large bias for large values of J . Such results guarantee the considerations in Remark 2 of Section

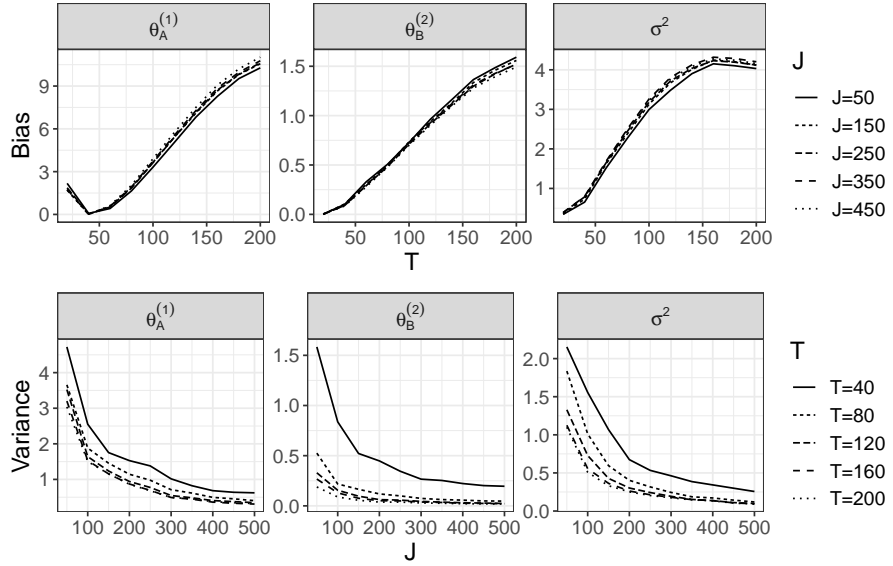


Figure 3: Simulation results for the distribution (a) with the normal covariate: Variations of the sample squared bias ($\times 10^3$) and variance ($\times 10^3$) of the proposed estimator with respect to J and T

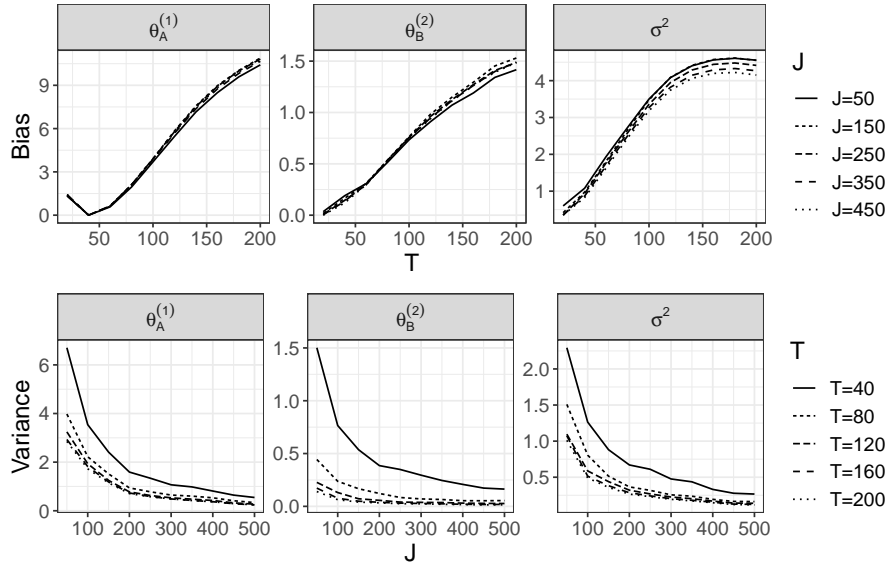


Figure 4: Simulation results for the distribution (a) with the uniform covariate: Variations of the sample squared bias ($\times 10^3$) and variance ($\times 10^3$) of the proposed estimator with respect to J and T

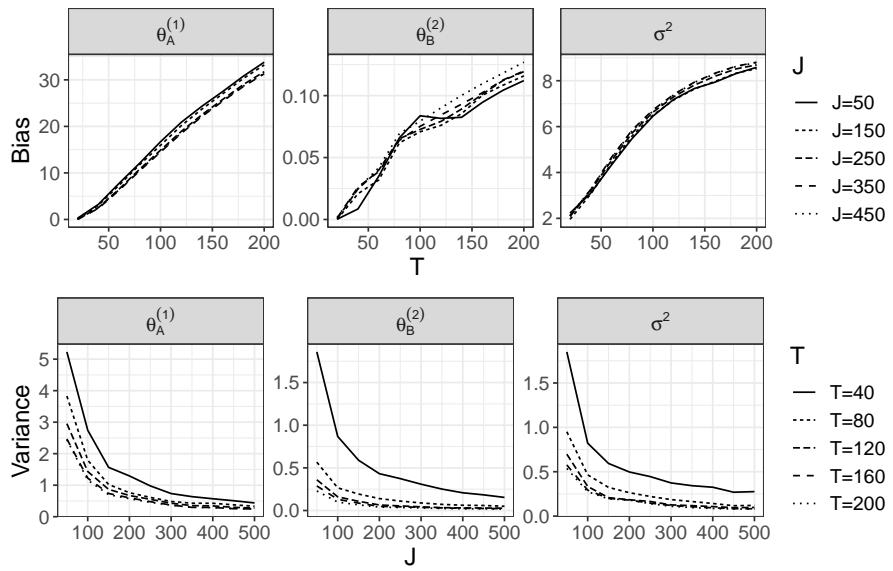


Figure 5: Simulation results for the distribution (b) with the normal covariate: Variations of the sample squared bias ($\times 10^3$) and variance ($\times 10^3$) of the proposed estimator with respect to J and T

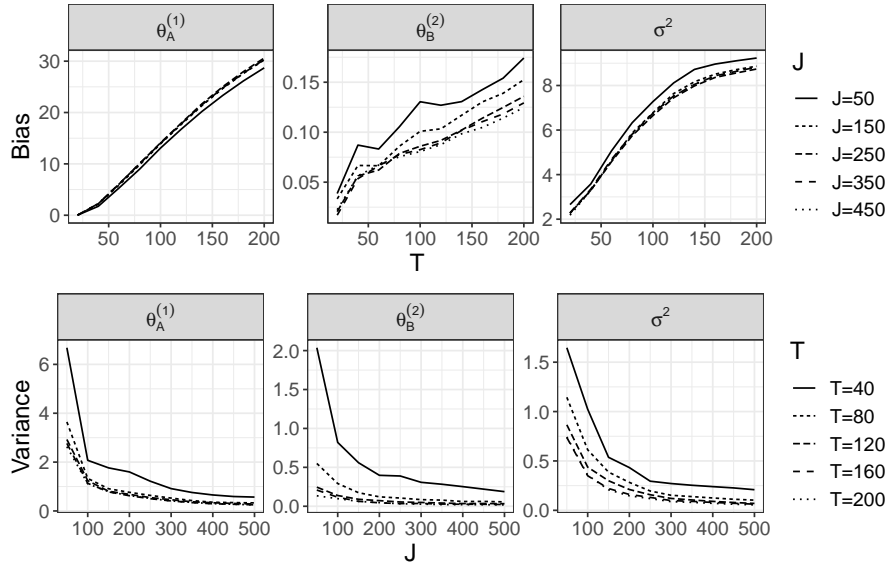


Figure 6: Simulation results for the distribution (b) with the uniform covariate: Variations of the sample squared bias ($\times 10^3$) and variance ($\times 10^3$) of the proposed estimator with respect to J and T

3.2. As described in Remark 1, from the second row of each figure, the variance of $\hat{\theta}_B^{(2)}$ was strongly dependent on both J and T when J was small, while the variances of $\hat{\theta}_A^{(1)}$ and $\hat{\sigma}^2$ were almost unaffected by T .

4.3 Borrowing of strength for extremes

In this section, we numerically compare our model, the fully parametric model (2), and the model proposed by Wang and Tsai (2009). Using the model proposed by Wang and Tsai (2009) implies that the areas are analyzed separately. For the latter two parametric models, we use the function `glm()` with `family=Gamma(link="log")` in the R to obtain their estimators.

Unlike Sections 4.1 and 4.2, the dataset is obtained from the fully parametric model (2) as follows. Let J be divided into $J = J^\dagger + J^\ddagger$. We set $J^\dagger = 130$, $J^\ddagger = 20$, $n_1 = \dots = n_{J^\dagger} = 100$ and $n_{J^\dagger+1} = \dots = n_{J^\dagger+J^\ddagger} = 20$. First, $X_{ij}^{(2)}$ is generated from $N(0, 1)$. Next, to generate Y_{ij} , we use the two distributions

$$F_j^\dagger(y | X_{ij}^{(2)}) = 1 - y^{-1/\gamma_j(X_{ij}^{(2)})}, \quad j = 1, \dots, J^\dagger \quad (17)$$

and

$$F_j^\ddagger(y | X_{ij}^{(2)}) = 1 - \frac{1.5y^{-1/\gamma_j(X_{ij}^{(2)})}}{1 + 0.5y^{-1/\gamma_j(X_{ij}^{(2)})}}, \quad j = J^\dagger + 1, \dots, J^\dagger + J^\ddagger \quad (18)$$

with the same (3), where F_j^\ddagger is described in detail in Section 4.1 of Wang and Tsai (2009). Then, (3) is modeled with $\mathbf{X}_{ij} = (X_{ij}^{(1)}, X_{ij}^{(2)})^\top$, $\mathbf{X}_{Aij} = X_{ij}^{(1)} \equiv 1$ and $\mathbf{X}_{Bij} = X_{ij}^{(2)}$, that is, $\gamma_j(X_{ij}^{(2)}) = \exp(\theta_{jA}^{(1)} + \theta_B^{(2)} X_{ij}^{(2)})$, where $\theta_B^{(2)} = 0.2$ and the parameters $\theta_{jA}^{(1)}$, $j \in \mathcal{J}$ are assigned the following two types. One $\theta_{jA}^{(1)}$ is defined as the $j/(J^\dagger + 1)$ -th quantile of $N(0, 1/12)$ for $j = 1, \dots, J^\dagger$ and $(j - J^\dagger)/(J^\ddagger + 1)$ -th quantile of $N(0, 1/12)$ for $j = J^\dagger + 1, \dots, J^\dagger + J^\ddagger$, and the other $\theta_{jA}^{(1)}$ is fixed as $-0.5 + 0.5(j - 1)/(J^\dagger - 1)$ for $j = 1, \dots, J^\dagger$ and $-0.5 + 0.5(j - J^\dagger - 1)/(J^\ddagger - 1)$ for $j = J^\dagger + 1, \dots, J^\dagger + J^\ddagger$. These two settings of $\theta_{jA}^{(1)}$ are denoted by Normal type and Uniform type, respectively.

Here, without introducing thresholds, we estimate $\theta_{jA}^{(1)}$, $j \in \mathcal{J}$ and $\theta_B^{(2)}$ by each of our model, the fully parametric model (2) and model proposed by Wang and Tsai (2009). For the model proposed by Wang and Tsai (2009), different estimates of $\theta_B^{(2)}$ are obtained across the areas, but the mean of these is used as the estimate of $\theta_B^{(2)}$. Under the above settings, if the areas were analyzed separately, the estimates from (18) would have large bias and variance values. Therefore, we are interested in whether these direct estimates can be improved by simultaneously analyzing the areas using the MEM. To verify this, we assess the sample bias and variance of the estimator for each method. Table 1 shows the results based on 500 sets of unit-level data, where the superscripts \dagger and \ddagger in this table refer to the means for $j = 1, \dots, J^\dagger$ and for $j = J^\dagger + 1, \dots, J^\dagger + J^\ddagger$, respectively. From Table 1, our model produced the most stable estimates among the three models. In particular, for θ_{jA} , $j = J^\dagger + 1, \dots, J^\dagger + J^\ddagger$, the variance of the estimates was dramatically improved using our model rather than the direct estimates. In addition, for EVT, we can see that the ‘‘borrowing of strength’’ of the MEM contributes to reducing the

Table 1: Sample bias and variance of the estimators for the three models

	Our model	Fully parametric model	Direct estimates
$\theta_{jA}^{(1)}$ (Normal type)			
Bias [†]	-1.77×10^{-3}	-4.39×10^{-3}	-9.50×10^{-3}
Bias [‡]	1.20×10^{-1}	1.77×10^{-1}	1.57×10^{-1}
Variance [†]	7.89×10^{-3}	9.97×10^{-3}	1.01×10^{-2}
Variance [‡]	1.69×10^{-2}	4.25×10^{-2}	4.59×10^{-2}
$\theta_{jA}^{(2)}$ (Uniform type)			
Bias [†]	2.00×10^{-1}	2.00×10^{-1}	2.00×10^{-1}
Bias [‡]	6.78×10^{-5}	6.78×10^{-5}	1.23×10^{-4}
Bias [†]	-3.07×10^{-3}	-5.56×10^{-3}	-1.06×10^{-2}
Bias [‡]	1.26×10^{-1}	1.80×10^{-1}	1.60×10^{-1}
Variance [†]	8.07×10^{-3}	9.98×10^{-3}	1.01×10^{-2}
Variance [‡]	1.73×10^{-2}	4.10×10^{-2}	4.50×10^{-2}
$\theta_{jB}^{(2)}$			
Bias	2.00×10^{-1}	2.00×10^{-1}	1.99×10^{-1}
Variance	7.32×10^{-5}	7.34×10^{-5}	1.13×10^{-4}

bias of the estimator. In the fully parametric model (2), the bias of the estimator was larger than that of the direct estimates. Meanwhile, even if the assumption of normality for random effects was not satisfied in (4), our model was still favorable.

5 Application

5.1 Background and dataset

5.1.1 Background

As an application, we analyze a real dataset of heavy rainfall in Japan for the period 2000-2022. From a global perspective, Japan is a country with significant rainfall, and heavy rains caused by seasonal fronts and typhoons often damage cities and affect residents. In particular, the heavy rainfall in western Japan in 2018 led to the worst damage in the period 2000-2022, killing a total of 225 people (Bandaru et al. 2020), and the damage was concentrated in the three prefectures of Okayama, Hiroshima, and Ehime. Figure 7 shows the time series plots of precipitation in these three prefectures, with the cross marks indicating the precipitation at that time. We can see from Figure 7 that the rainfall at that time was extreme, which implies that such unforeseen events may cause severe damage. Despite this background, there are limited findings on applying extreme value analysis to heavy rainfall events in Japan. We are interested in the tail behavior of the distribution of extreme precipitation at various sites in Japan.

5.1.2 Dataset

The dataset is obtained from the Japan Meteorological Agency website (<https://www.data.jma.go.jp/g>). Here, we cover all 155 weather stations for which daily total precipitation (mm), daily mean wind speed (m/s) and daily mean vapor pressure (hPa) are available.

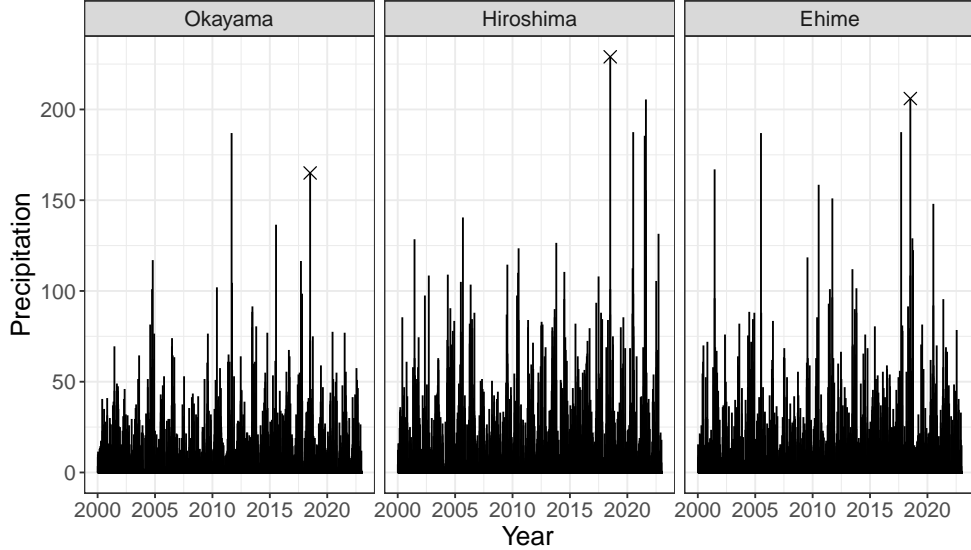


Figure 7: Time series plots of precipitation in Okayama, Hiroshima, and Ehime prefectures. In each panel, the cross mark indicates the precipitation of the heavy rains in western Japan in 2018

Figure 8 shows the locations of all the stations, where the symbols in this figure are explained in Section 5.2.1. In this dataset, at each of the 150 stations, we can use over 8,000 daily observations from 2000 to 2022. The remaining five stations have 5,732, 5,744, 7,052, 7,915, and 7,984 days of observations during the same period, respectively.

In the following Sections 5.2-5.5, we assume that all the observations at one weather station form one area. Accordingly, our dataset can be organized into unit-level data as (1), where Y_{ij} denotes daily precipitation, and $\mathbf{X}_{ij} := (X_{ij}^{(1)}, X_{ij}^{(2)}, X_{ij}^{(3)})^\top \in \mathbb{R}^3$ is composed of $X_{ij}^{(1)} \equiv 1$ and the daily wind speed $X_{ij}^{(2)}$ and vapor pressure $X_{ij}^{(3)}$.

By convention, $\{X_{ij}^{(2)}\}_{i \in \mathcal{N}_j, j \in \mathcal{J}}$ and $\{X_{ij}^{(3)}\}_{i \in \mathcal{N}_j, j \in \mathcal{J}}$ are standardized to have zero sample mean and unit unbiased sample variance. To locate a particular station from the map in Figure 8, each of the 151 stations, excluding the triangles in Figure 8, is assigned an index j from 1 to 151 in order of latitude. Thus, the southernmost and northernmost stations are labeled $j = 1$ and $j = 151$, respectively. By the same rule, the four stations indicated by the triangles in Figure 8 have the indices $j = 152, 153, 154, 155$.

Our goal is to apply our method to this dataset and confirm its efficiency. In particular, we aim to investigate whether the proposed MEM, which combines all areas, performs better than the estimates obtained directly from each area. Before doing so, we must verify some of the assumptions used in our model.

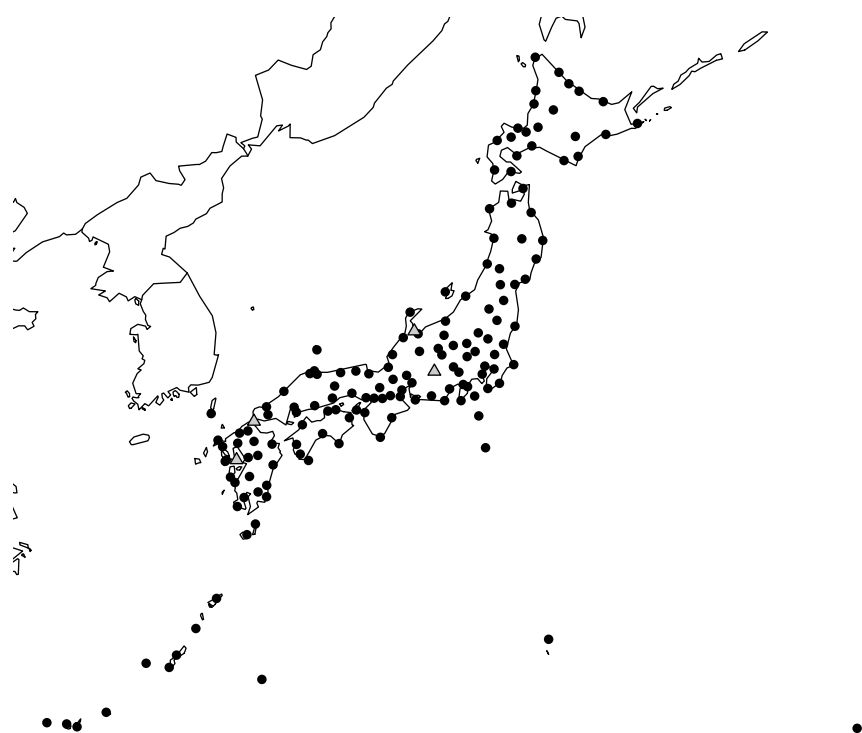


Figure 8: Map of Japan showing the locations of the 155 available weather stations (areas), where both the dots and triangles mark the locations

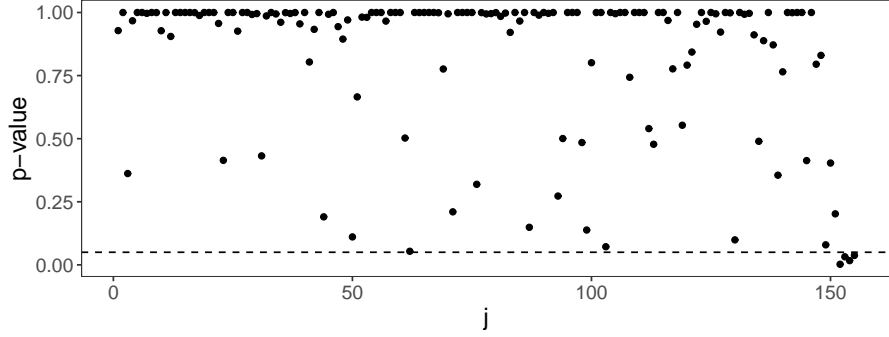


Figure 9: The p-value of the test (19) for each of the 155 stations

5.2 Preliminary Analysis

5.2.1 Positivity of extreme value index

The key assumptions in our model (5) with (6) are the use of the Pareto-type distribution and acceptance of heterogeneity among the areas. To verify whether these assumptions are reasonable for our dataset, we apply the GPD using the generalized additive model (GAM) separately for each of the 155 stations (Youngman 2019). Then, at the j th station, for a given sufficiently high threshold $\omega_j^{\text{GPD}} > 0$, the exceedances $Y_{ij} - \omega_j^{\text{GPD}}$, $i \in \mathcal{N}_j$ are modeled as

$$\begin{aligned} P(Y_{ij} - \omega_j^{\text{GPD}} \leq y \mid \mathbf{X}_{ij} = \mathbf{x}, Y_{ij} > \omega_j^{\text{GPD}}) \\ = 1 - \left(1 + \gamma_j^{\text{GPD}} \frac{y}{\psi_j(\mathbf{x})} \right)^{-1/\gamma_j^{\text{GPD}}} \end{aligned}$$

for $\mathbf{x} := (x^{(1)}, x^{(2)}, x^{(3)})^\top \in \mathbb{R}^3$ and $y \in \{y : y > 0 \text{ and } \gamma_j^{\text{GPD}} y / \psi_j(\mathbf{x}) > 0\}$ with the scale parameter $\psi_j(\mathbf{x}) > 0$ and EVI $\gamma_j^{\text{GPD}} \in \mathbb{R}$, where the GAM is employed to $\psi_j(\mathbf{x})$ as

$$\begin{aligned} \log(\psi_j(\mathbf{x})) &= a_j, \\ \log(\psi_j(\mathbf{x})) &= a_j + s_j^{(2)}(x^{(2)}), \\ \log(\psi_j(\mathbf{x})) &= a_j + s_j^{(3)}(x^{(3)}) \quad \text{or} \\ \log(\psi_j(\mathbf{x})) &= a_j + s_j^{(2)}(x^{(2)}) + s_j^{(3)}(x^{(3)}), \end{aligned}$$

where a_j is an unknown parameter, and $s_j^{(2)}(\cdot)$ and $s_j^{(3)}(\cdot)$ are unknown univariate nonparametric functions.

Under the above model, we first conduct the following hypothesis test on the sign of the EVI γ_j^{GPD} :

$$H_{0j}^{\text{GPD}} : \gamma_j^{\text{GPD}} > 0 \quad \text{vs.} \quad H_{1j}^{\text{GPD}} : \gamma_j^{\text{GPD}} \leq 0, \quad (19)$$

where H_{0j}^{GPD} is the null hypothesis, and H_{1j}^{GPD} is the alternative hypothesis. That is, we want to exclude areas that have a high probability of negative EVI. Now, let $\hat{\gamma}_j^{\text{GPD}}$ be the estimator of γ_j^{GPD} using the package `evgam` (Youngman 2022) within

the \mathbf{R} , where the threshold ω_j^{GPD} and one of four models of $\psi_j(\mathbf{x})$ are chosen in terms of the GPD version of the discrepancy measure. From the test statistics given in Section 3.1 of Einmahl et al. (2019) and asymptotic result of GPD-GAM shown in Theorem 4 of Yoshida (2023), for a significance level α , the null hypothesis H_{0j}^{GPD} is rejected if $(n_{j0}^{\text{GPD}})^{1/2} \hat{\gamma}_j^{\text{GPD}} \leq z_\alpha$, where $n_{j0}^{\text{GPD}} := \sum_{i=1}^{n_j} I(Y_{ij} > \omega_j^{\text{GPD}})$, and z_α is the 100α -th percentile point of $N(0, 1)$. As a result of applying the test (19) with $\alpha = 0.05$ to each of the 155 stations, the null hypothesis H_{0j}^{GPD} was rejected for only four stations indicated by triangles in Figure 8. Figure 9 shows the p-values of the test (19) for all the stations. Thus, the result suggests that the EVI of the distribution of extreme precipitation is positive or close to zero in most stations in Japan.

5.2.2 Heterogeneity of EVI

We next examine the heterogeneity of the EVIs γ_j^{GPD} , $j = 1, 2, \dots, 151$ of the 151 stations for which the null hypothesis H_{0j}^{GPD} was not rejected in (19). To achieve this, we consider the hypothesis test, where the null and alternative hypotheses are expressed as follows:

$$\begin{aligned} H_0^{\text{GPD}} : & \forall j_1, \forall j_2 \in \{1, 2, \dots, 151\}, \gamma_{j_1}^{\text{GPD}} = \gamma_{j_2}^{\text{GPD}} \\ \text{vs. } H_1^{\text{GPD}} : & \exists j_1, \exists j_2 \in \{1, 2, \dots, 151\} \text{ s.t. } \gamma_{j_1}^{\text{GPD}} \neq \gamma_{j_2}^{\text{GPD}}. \end{aligned} \quad (20)$$

According to Section 3.2 of Einmahl et al. (2019) and Theorem 4 of Yoshida (2023), the test statistic is given by

$$T := \sum_{j=1}^{151} \frac{n_{j0}^{\text{GPD}}}{\left(1 + \hat{\gamma}_j^{\text{GPD}}\right)^2} \left(\hat{\gamma}_j^{\text{GPD}} - \bar{\gamma}^{\text{GPD}}\right)^2,$$

where $\bar{\gamma}^{\text{GPD}} := [\sum_{j=1}^{151} \{n_{j0}^{\text{GPD}} / (1 + \hat{\gamma}_j^{\text{GPD}})^2\}]^{-1} \sum_{j=1}^{151} \{n_{j0}^{\text{GPD}} \hat{\gamma}_j^{\text{GPD}} / (1 + \hat{\gamma}_j^{\text{GPD}})^2\}$. For a significance level α , we will reject the null hypothesis H_0^{GPD} if the test statistic T is outside of the $100\alpha/2$ -th and $100(1 - \alpha/2)$ -th percentile points of the chi-squared distribution with 150 degrees of freedom. As a result of applying the test (20), the null hypothesis H_0^{GPD} was rejected for the given $\alpha = 0.05$, and the p-value for the obtained $T = 965$ was less than 10^{-6} . Therefore, the EVI varies significantly across the 151 stations.

The results of the above two tests (19) and (20) motivate us to use our Pareto-type model (5) with (6) rather than the GPD. In the following Sections 5.3-5.5, we analyze the data only for the 151 weather stations for which the null hypothesis H_{0j}^{GPD} was not rejected in (19). Accordingly, the number of areas is changed to $J = 151$.

5.3 Analysis by our model

5.3.1 Partition of covariates

We apply the proposed model (5) with (6) to the dataset. Throughout Sections 5.3 and 5.4, some of the results are presented only for the areas with $j = 6, 13, 22$,

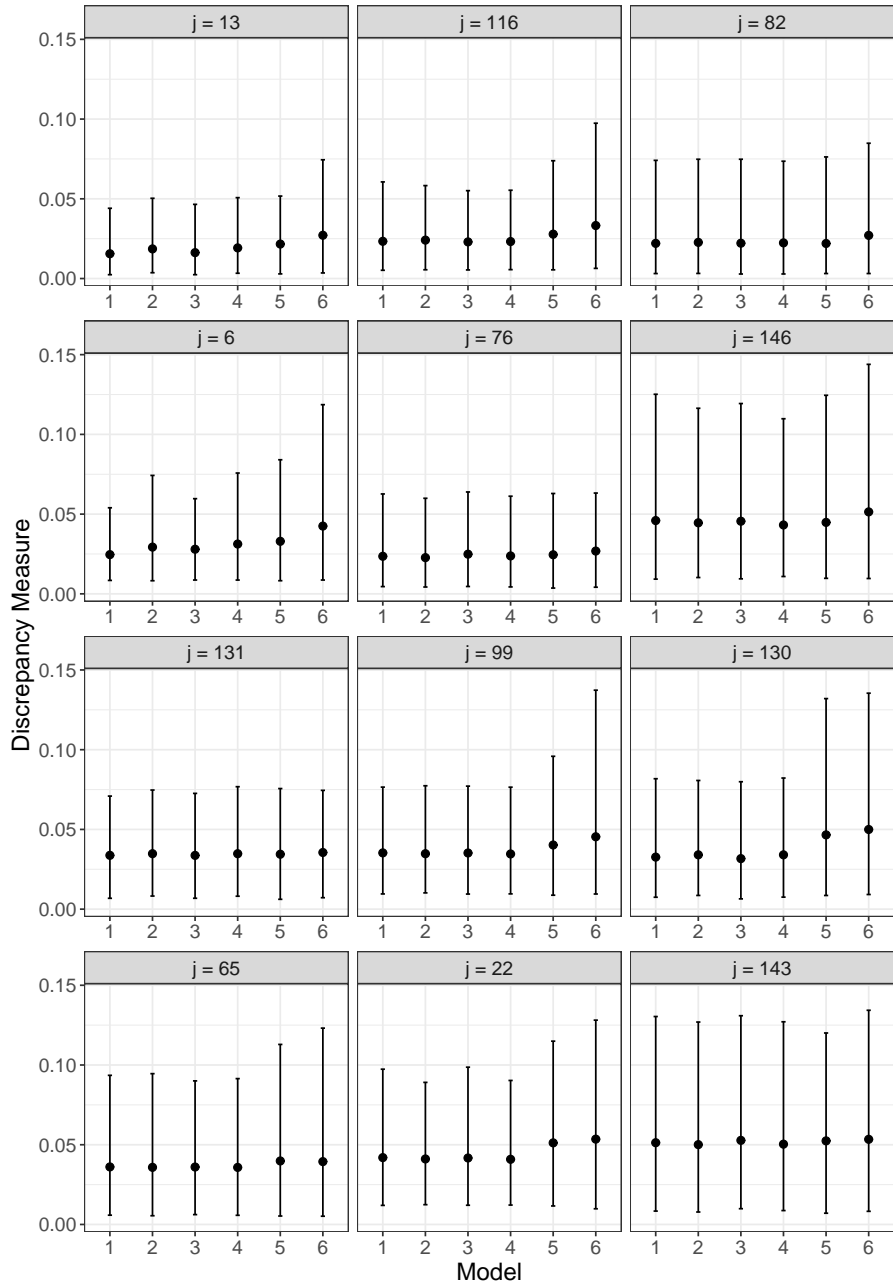


Figure 10: The 5th and 95th percentiles (lines) and mean (dots) of the replicates of the discrepancy measure for each of the 12 representative stations. The labels “1”, “2”, “3”, “4”, “5” and “6” on the horizontal axis refer to the models (21)-(24), fully parametric model (2) and direct area estimator, respectively

65, 76, 82, 99, 116, 130, 131, 143, 146, where these representatives were carefully selected in Section 5.3.3.

We begin by setting up our model. If we take the model (6) for (5), $\mathbf{X}_{ij} = (X_{ij}^{(1)}, X_{ij}^{(2)}, X_{ij}^{(3)})^\top = (1, X_{ij}^{(2)}, X_{ij}^{(3)})^\top$ can be partitioned into \mathbf{X}_{Aij} and \mathbf{X}_{Bij} as

$$\mathbf{X}_{Aij} = X_{ij}^{(1)} \equiv 1 \quad \text{and} \quad \mathbf{X}_{Bij} = (X_{ij}^{(2)}, X_{ij}^{(3)}), \quad (21)$$

$$\mathbf{X}_{Aij} = (X_{ij}^{(1)}, X_{ij}^{(2)})^\top \quad \text{and} \quad \mathbf{X}_{Bij} = X_{ij}^{(3)}, \quad (22)$$

$$\mathbf{X}_{Aij} = (X_{ij}^{(1)}, X_{ij}^{(3)})^\top \quad \text{and} \quad \mathbf{X}_{Bij} = X_{ij}^{(2)}, \quad \text{or} \quad (23)$$

$$\mathbf{X}_{Aij} = (X_{ij}^{(1)}, X_{ij}^{(2)}, X_{ij}^{(3)})^\top \quad \text{and} \quad \mathbf{X}_{Bij} \equiv 0. \quad (24)$$

Among the above four models, we select the one that best fits our dataset. To do this, we iterate the computation of the following 2-fold cross-validation criteria. At each iteration, the observations for each station are divided randomly and equally into training and test data. Subsequently, for each of the models (21)-(24), the discrepancy measure for each station is computed for the test data using the estimated parameters, predicted random effects, and selected thresholds from training data. Through a total of 100 iterations, we obtain 100 replicates of the discrepancy measure for each of the stations for each of the models (21)-(24). Figure 10 shows the obtained replicates in terms of 5th and 95th percentiles (lines) and mean (dots) for the 12 representative stations, where, the labels “1”, “2”, “3” and “4” on the horizontal axis refer to the models (21), (22), (23) and (24), respectively. According to Figure 10, the discrepancy measures did not differ significantly between the models (21)-(24). In addition, the mean of the discrepancy measures over all 151 stations was 0.02805 for (21), 0.02812 for (22), 0.02827 for (23), and 0.02828 for (24). Therefore, we can adequately reflect the structure of our dataset with the nested error regression type model (21), without using the more complicated models (22)-(24). Therefore, we present the results of the analysis for our dataset, focusing on (21).

5.3.2 Main results for our model

Let us set $\mathbf{X}_{Aij} = X_{ij}^{(1)} \equiv 1$ and $\mathbf{X}_{Bij} = (X_{ij}^{(2)}, X_{ij}^{(3)})^\top$ and denote the random effects (4) as $U_1, U_2, \dots, U_J \sim N(0, \sigma^2)$, where $\sigma^2 > 0$ is an unknown variance parameter. For the conditional response distribution (5), the EVI is modeled as follows:

$$\gamma(u_j, x^{(2)}, x^{(3)}) = \exp \left(\theta_A^{(1)} + u_j + \theta_B^{(2)} x^{(2)} + \theta_B^{(3)} x^{(3)} \right) \quad (25)$$

for given $U_j = u_j$, $X_{ij}^{(2)} = x^{(2)}$ and $X_{ij}^{(3)} = x^{(3)}$, where $\theta_A^{(1)}$, $\theta_B^{(2)}$ and $\theta_B^{(3)}$ are unknown regression coefficients.

First, we estimate the parameters $\{\theta_A^{(1)}, \theta_B^{(2)}, \theta_B^{(3)}, \sigma^2\}$ using the method proposed in Section 2. The selected ω_j and n_{j0} , $j \in \mathcal{J}$ are shown in Table 2, where the mean of n_{j0} , $j \in \mathcal{J}$ is about 100, and this value was used in the simulation of Section 4. Then, the parameters were obtained as follows:

$$\hat{\theta}_A^{(1)} = -1.4618, \quad \hat{\theta}_B^{(2)} = 0.1061, \quad \hat{\theta}_B^{(3)} = 0.2854 \quad \text{and} \quad \hat{\sigma}^2 = 0.0799.$$

The positivity of $\hat{\theta}_B^{(2)}$ and $\hat{\theta}_B^{(3)}$ can be interpreted as, the larger $X_{ij}^{(2)}$ and $X_{ij}^{(3)}$, the heavier the right tail of the distribution of extreme precipitation. This is a natural

Table 2: Selected threshold ω_j , number of threshold exceedances n_{j0} and predicted EVI γ_j^* for each station

j	n_{j0}	ω_j	γ_j^*	j	n_{j0}	ω_j	γ_j^*	j	n_{j0}	ω_j	γ_j^*
1	17	88	0.37	52	238	26	0.47	103	22	83	0.24
2	265	46	0.58	53	56	78	0.26	104	146	44	0.38
3	42	120	0.41	54	83	64	0.31	105	33	88	0.19
4	68	91	0.37	55	32	68	0.24	106	82	35	0.32
5	42	120	0.35	56	77	86	0.33	107	134	49	0.30
6	80	72	0.44	57	111	60	0.36	108	310	38	0.52
7	41	134	0.34	58	35	90	0.34	109	93	56	0.35
8	157	68	0.38	59	33	70	0.23	110	89	62	0.24
9	35	126	0.35	60	128	43	0.33	111	54	62	0.32
10	48	78	0.28	61	121	38	0.35	112	136	46	0.36
11	34	112	0.35	62	49	66	0.31	113	69	43	0.30
12	37	132	0.32	63	82	66	0.34	114	23	78	0.27
13	122	130	0.34	64	74	118	0.32	115	190	34	0.36
14	105	84	0.40	65	22	120	0.25	116	61	51	0.33
15	62	112	0.28	66	41	71	0.29	117	151	30	0.41
16	17	160	0.23	67	55	58	0.33	118	63	64	0.30
17	38	137	0.31	68	53	72	0.29	119	52	58	0.28
18	94	101	0.34	69	56	84	0.31	120	265	30	0.37
19	53	123	0.30	70	132	79	0.34	121	95	46	0.33
20	23	149	0.29	71	197	50	0.37	122	118	61	0.32
21	56	102	0.32	72	221	37	0.39	123	32	98	0.31
22	9	190	0.24	73	73	86	0.32	124	74	49	0.29
23	31	157	0.30	74	274	30	0.42	125	253	30	0.38
24	61	104	0.31	75	162	54	0.37	126	117	38	0.39
25	120	89	0.38	76	78	71	0.36	127	44	60	0.32
26	43	97	0.30	77	195	42	0.35	128	114	34	0.38
27	204	48	0.48	78	59	58	0.28	129	26	78	0.21
28	18	206	0.25	79	29	94	0.22	130	24	60	0.22
29	74	88	0.37	80	258	31	0.43	131	126	33	0.35
30	285	58	0.41	81	89	71	0.33	132	54	51	0.27
31	274	42	0.49	82	205	38	0.39	133	39	96	0.28
32	134	55	0.38	83	85	57	0.34	134	26	70	0.25
33	160	52	0.43	84	139	44	0.33	135	138	40	0.39
34	60	108	0.33	85	288	32	0.52	136	46	44	0.29
35	60	95	0.34	86	225	37	0.37	137	154	28	0.33
36	79	76	0.34	87	143	44	0.38	138	89	38	0.34
37	54	114	0.28	88	128	48	0.39	139	82	48	0.31
38	73	113	0.31	89	36	76	0.25	140	102	34	0.31
39	32	162	0.25	90	83	50	0.35	141	127	30	0.31
40	17	126	0.26	91	89	64	0.35	142	63	43	0.28
41	49	88	0.36	92	54	82	0.30	143	11	90	0.23
42	116	51	0.33	93	120	49	0.47	144	58	41	0.31
43	32	132	0.34	94	30	70	0.24	145	61	36	0.34
44	123	137	0.45	95	41	78	0.25	146	54	41	0.32
45	35	139	0.30	96	106	48	0.36	147	9	77	0.24
46	77	79	0.30	97	164	39	0.42	148	22	58	0.26
47	143	82	0.34	98	144	46	0.35	149	47	46	0.32
48	46	69	0.42	99	113	54	0.39	150	185	25	0.44
49	28	85	0.26	100	64	44	0.31	151	152	25	0.40
50	144	35	0.42	101	279	25	0.42				
51	232	37	0.53	102	49	70	0.29				

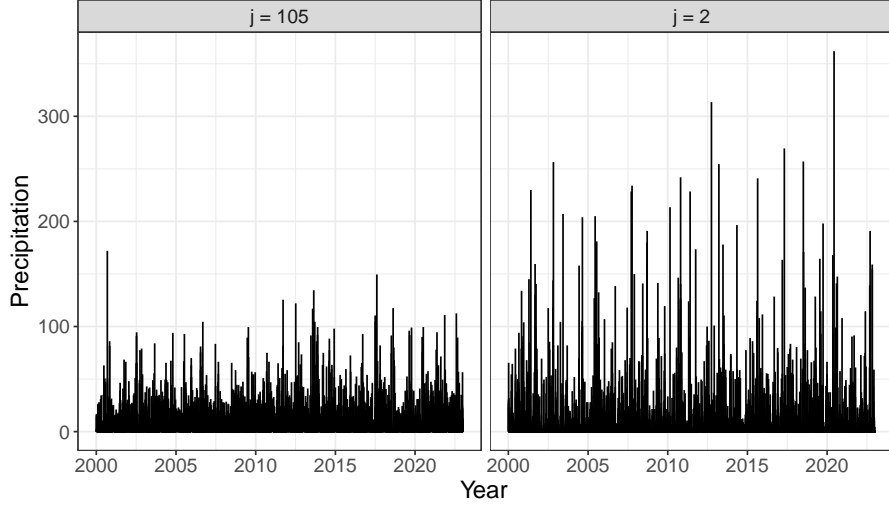


Figure 11: Time series plots of precipitation at the 2nd and 105th stations

result because the high values of $X_{ij}^{(2)}$ and $X_{ij}^{(3)}$ tend to occur during typhoon or rainy season.

Secondly, we perform the Wald hypothesis tests based on Corollary 1. The hypothesis tests of interest are expressed as follows:

$$H_{0k} : \theta_B^{(k)} = 0 \quad \text{vs.} \quad H_{1k} : \theta_B^{(k)} \neq 0$$

for $k \in \{2, 3\}$, where H_{0k} is the null hypothesis and H_{1k} is the alternative hypothesis. From Corollary 1, we define the test statistic as

$$T_k := (\boldsymbol{\Omega}_B)_{k-p_A}^{-1/2} \left\{ (Jn_0)^{1/2} \hat{\theta}_B^{(k)} - (\mathbf{v}_B)_{k-p_A} \right\}, \quad k \in \{2, 3\},$$

where $(\boldsymbol{\Omega}_B)_{k-p_A}$ is the $(k-p_A, k-p_A)$ entry of the matrix $\boldsymbol{\Omega}_B$, and $(\mathbf{v}_B)_{k-p_A}$ is the $(k-p_A)$ -th component of the vector \mathbf{v}_B . Under the null hypothesis H_{0k} , the distribution of T_k can be approximated by $N(0, 1)$. Here, $\boldsymbol{\Omega}_B^{-1}$ is estimated by (14), and it is assumed that \mathbf{v}_B is a zero vector. Then, for a significance level α , we reject the null hypothesis H_{0k} if $|T_k| > z_{1-\alpha/2}$. As the results with $\alpha = 0.05$, the test statistics were $T_2 = 16.92$ and $T_3 = 21.35$, and the p-values for $k = 2, 3$ were less than 10^{-6} . Thus, the null hypothesis H_{0k} was rejected for both $\theta_B^{(2)}$ and $\theta_B^{(3)}$. Therefore, the effects of wind speed and vapor pressure may not be ignored.

Finally, we predict the EVI for each of the 151 stations based on the model (25). To capture the variation in $\gamma(u_j, x^{(2)}, x^{(3)})$ with respect to only j , we use

$$\gamma_j^* := \frac{1}{n_{j0}} \sum_{i=1}^{n_j} \exp \left(\hat{\theta}_A^{(1)} + \tilde{u}_j + \hat{\theta}_B^{(2)} X_{ij}^{(2)} + \hat{\theta}_B^{(3)} X_{ij}^{(3)} \right) I(Y_{ij} > \omega_j), \quad (26)$$

where \tilde{u}_j is the predictor of U_j calculated by (11). The last column of Table 2 shows the obtained γ_j^* , $j = 1, 2, \dots, 151$, where the maximum and minimum values were reached at the 2nd and 105th stations, respectively. Figure 11 shows the time series plots of precipitation at the 2nd and 105th stations. A station with a high EVI is considered hazardous, as it has a higher probability of witnessing precipitation

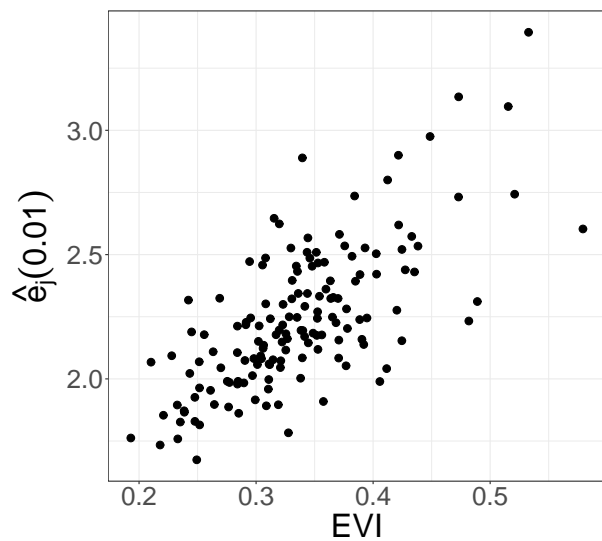


Figure 12: Plot of $\hat{e}_j(0.001, 0.01)$ against γ_j^*

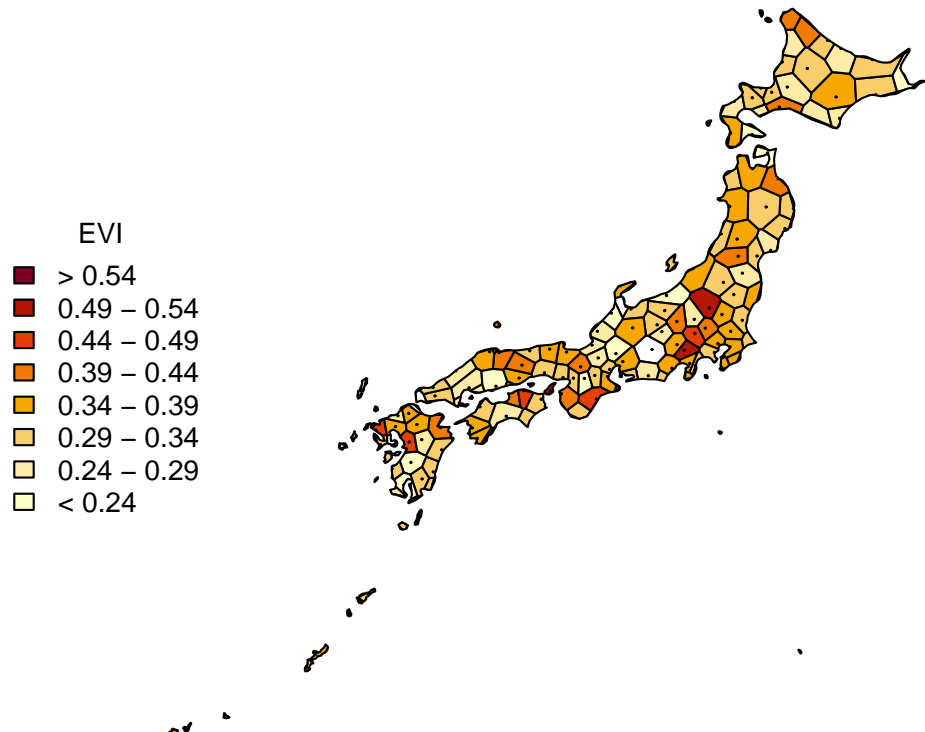


Figure 13: Heatmap of the EVI $\gamma_j^*, \in \mathcal{J}$

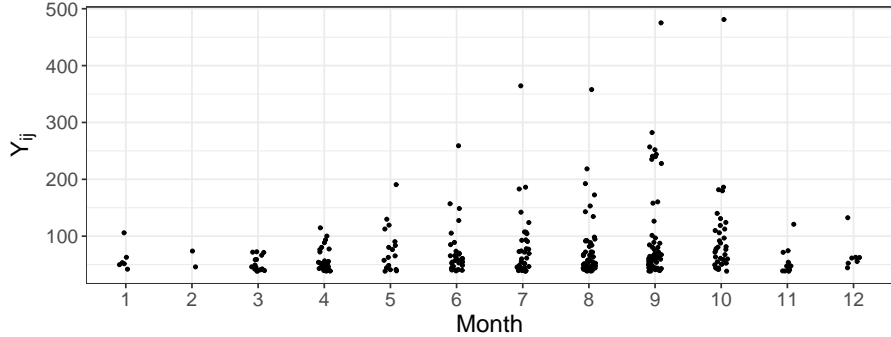


Figure 14: Plot of the threshold exceedances $\{Y_{ij} : Y_{ij} > \omega_j, i \in \mathcal{N}_j, j = 108\}$ by month

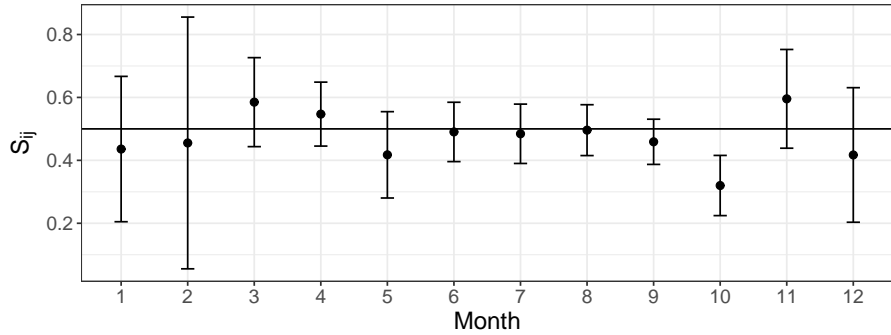


Figure 15: Mean of \mathcal{S}_{108} by month and its 95 % confidence interval computed using the central limit theorem

levels that surpass its historical records. To verify this, we compare two different return levels of precipitation as follows:

$$\hat{e}_j(p_1, p_2) := \frac{\hat{Q}_j(1 - p_2)}{\hat{Q}_j(1 - p_1)}, \quad j = 1, 2, \dots, 151,$$

where $\hat{Q}_j(\cdot)$ is the empirical quantile function of $\{Y_{ij}\}_{i \in \mathcal{N}_j}$. Figure 12 is the plot of $\hat{e}_j(0.01, 0.001)$ against γ_j^* , where $\hat{e}_j(0.01, 0.001)$ is the ratio of the 100 day and 1000 day return levels of precipitation. There is a relatively strong correlation between γ_j^* and $\hat{e}_j(0.01, 0.001)$, with a correlation coefficient 0.70. As shown in Figure 12, the magnitudes of ordinary heavy rain $\hat{Q}_j(1 - p_1)$ and rare heavy rain $\hat{Q}_j(1 - p_2)$ differ significantly in proportion to the EVI γ_j^* . Meanwhile, Figure 13 shows the heatmap of γ_j^* , $j \in \mathcal{J}$, where the four stations for which the null hypothesis H_{j0}^{GPD} was not rejected in Section 5.2.1 are shown in white. In this figure, the boundaries are constructed by the package `deldir` (<https://CRAN.R-project.org/package=deldir>) within the R. From Figure 13, stations with high EVIs seem to be concentrated around Tokyo, the capital of Japan.

5.3.3 Goodness of fit

In this section, we concentrate on examining the adequacy of the model (25).

Figure 14 shows the plot of the threshold exceedances $\{Y_{ij} : Y_{ij} > \omega_j, i \in \mathcal{N}_j, j = 108\}$ by month. According to Figure 14, August and September have more precipitation than January and February, and the distribution of heavy precipitation includes seasonality as an important feature. Therefore, we must verify whether such seasonality is sufficiently incorporated into the model via the covariates $X_{ij}^{(2)}$ and $X_{ij}^{(3)}$. Now, from (8), the distribution of $S_{ij} := \exp\{-\gamma(U_j, X_{ij}^{(2)}, X_{ij}^{(3)})^{-1} \log(Y_{ij}/\omega_j)\}$ conditional on $U_j, X_{ij}^{(2)}, X_{ij}^{(3)}$ and $Y_{ij} > \omega_j$ can be approximated by the uniform distribution on $[0, 1]$ (Wang and Tsai 2009). Let \hat{S}_{ij} be S_{ij} replacing $(\theta_A^{(1)}, \theta_B^{(2)}, \theta_B^{(3)})$ and U_j by $(\hat{\theta}_A^{(1)}, \hat{\theta}_B^{(2)}, \hat{\theta}_B^{(3)})$ and \tilde{u}_j , respectively. Then, each of $\mathcal{S}_j := \{\hat{S}_{ij} : Y_{ij} > \omega_j, i \in \mathcal{N}_j\}, j = 1, 2, \dots, 151$ can be considered as approximated i.i.d. random samples from the uniform distribution on $[0, 1]$. Therefore, we can examine the seasonality problem using \mathcal{S}_j . The station mentioned above with $j = 108$ is particularly suitable for evaluating the results because it has the most threshold exceedances. Figure 15 shows the mean of \mathcal{S}_{108} by month and its 95 % confidence interval computed using the central limit theorem. From Figure 15, we can see that the standardized Y_{ij} using $X_{ij}^{(2)}$ and $X_{ij}^{(3)}$ has no seasonality except in October. Therefore, it can be recognized that our model (25) reflects the seasonality of heavy rainfall almost effectively.

Meanwhile, the above \mathcal{S}_j is also useful for evaluating the goodness of fit of the model. Figure 16 shows the Q-Q plot for \mathcal{S}_j against equally divided points on $[0, 1]$ for each of the 12 representative stations, where the bands are the 95% pointwise confidence bands described in Section 4.1. These representative stations with $j = 13, 116, 82, 6, 76, 146, 131, 99, 130, 65, 22, 143$ had the 1st, 20th, 38th, 57th, 76th, 95th, 114th, 132nd, 140th, 144th, 150th, and 151st largest values of the discrepancy measures computed from \mathcal{S}_j , respectively. Note that $\{1, 20, 38, 57, 76, 95, 114, 132, 151\}$ are equally divided points from 1 to 151. From Figure 16, at numerous stations, the points were aligned on a straight line with an intercept of 0 and slope of 1, indicating that the proposed model fits our dataset well.

5.4 Comparison

From the first column of Table 2, the sample size of threshold exceedances n_{j0} is now below 30 at 18 stations. At such stations with small effective sample sizes, estimates are expected to be unstable. However, from the Q-Q plots in Figure 16, our dataset contains many stations where most of the data fits the Pareto distribution as (8). This overall situation resulting from the peak over threshold method is similar to that in which the “borrowing of strength” of the MEM works well, as described in Section 4.3. The descriptions of “5” and “6” in Figure 10 show the results for the fully parametric model (2) and model proposed by Wang and Tsai (2009) with $\mathbf{X}_{Aij} = X_{ij}^{(1)}$ and $\mathbf{X}_{Bij} = (X_{ij}^{(2)}, X_{ij}^{(3)})^\top$. The mean of the discrepancy measures over all stations is 0.03226 for “5” and 0.03540 for “6”, which are slightly higher than that of the proposed model “1” as 0.02805 shown in Section 5.3.1. From Figure 10, we can see that at many stations, our model (21) yielded significantly smaller discrepancy measures than the two models “5” and “6.” This result indicates that our model (21) provided the most stable and least biased estimates, as described in

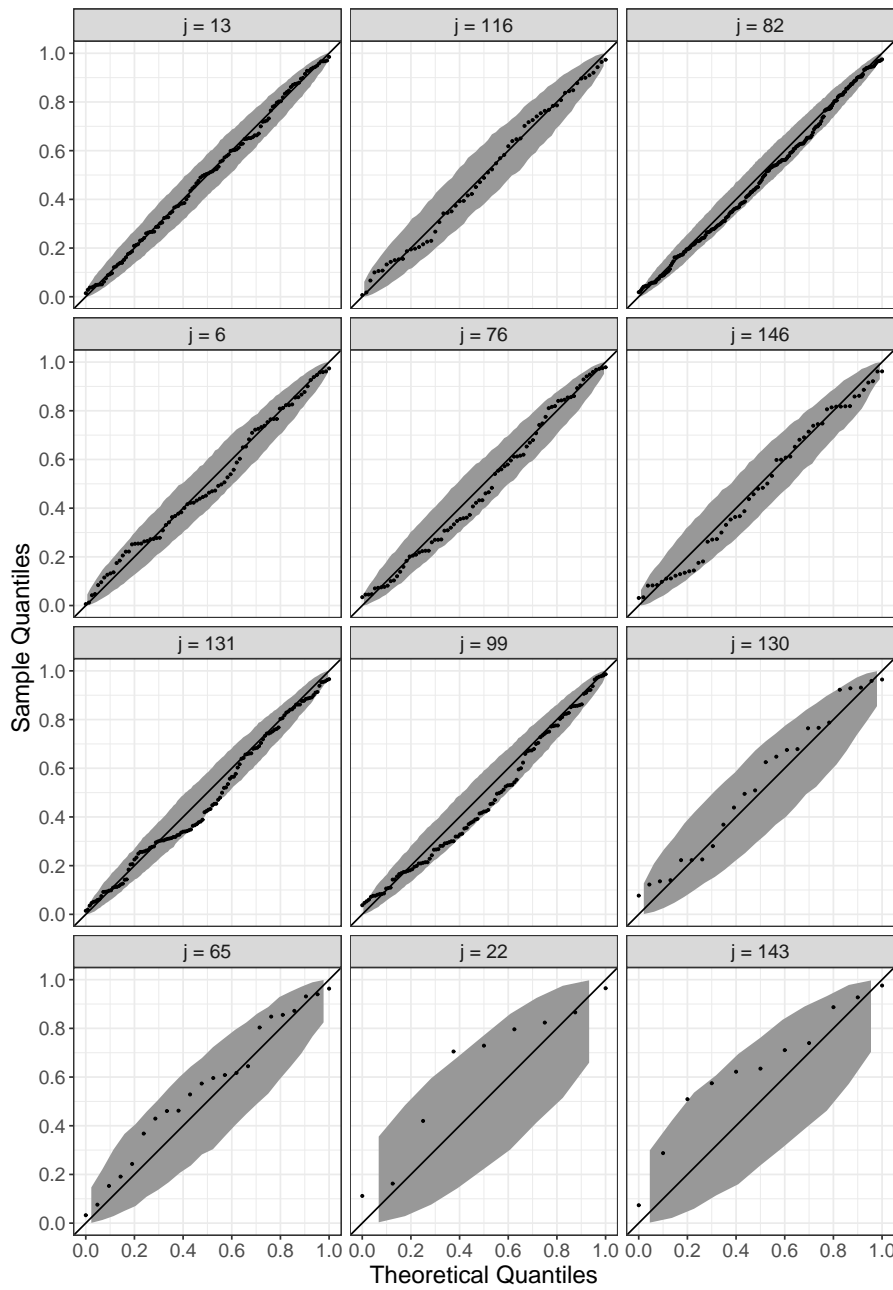


Figure 16: Q-Q plot for \mathcal{S}_j against equally divided points on $[0, 1]$ for each of the 12 representative stations

Section 4.3.

Next, we examine the sensitivity of the results to the choice of thresholds. The goal is to evaluate the effect of changing the threshold on the EVI γ_j^* of that particular station. To facilitate the interpretation of the results, we compare our model “1”, the fully parametric model “5” and the direct estimator “6” using the model proposed by Wang and Tsai (2009), where for the models “5” and “6”, γ_j^* is obtained by the same rule as (26). Figure 17 shows the plot of ω_j versus γ_j^* for each of the 12 representative stations, where the vertical line in each panel is the threshold selected by the discrepancy measure. From Figure 17, we can see that our model produced the most stable γ_j^* near the vertical line. In other words, our model is less sensitive to the choice of thresholds because it can reduce the instability of estimates at high thresholds.

5.5 Future Analysis

In Sections 4.3 and 5.4, we illustrated the advantages of using the MEM rather than analyzing the areas separately. Although we examined the standard MEM in this study, extending it to more sophisticated models may provide more detailed results for the dataset we analyzed. In the following, we discuss future work on the analysis of our dataset.

One of the essential issues is the dependencies between stations. To investigate their existence, we use

$$\gamma_{ij} := \exp \left(\hat{\theta}_A^{(1)} + \tilde{u}_j + \hat{\theta}_B^{(2)} X_{ij}^{(2)} + \hat{\theta}_B^{(3)} X_{ij}^{(3)} \right).$$

If the mean of γ_{ij} for each year from 2000 to 2022 is strongly correlated for two different stations, some dependence might exist between these stations because they share the same annual trend of γ_{ij} . Each panel of Figure 18 shows the plot of the annual mean of γ_{ij} for two particular stations. The upper panels provide examples of two geographically adjacent stations, where the given two examples had strong and weak correlations of the annual means of γ_{ij} , respectively. The correlation coefficients for these examples were obtained as 0.83 and 0.13, respectively. In contrast, the lower panels give examples of two geographically distant stations, where the correlation coefficients for the given two examples are 0.90 and 0.35, respectively. The results suggest the existence of dependencies between some stations. However, such dependencies between stations may not be determined by distance alone. The advantage of the MEM is that the number of parameters is independent of the number of areas J . Consequently, it is difficult to incorporate dependencies between stations (areas) directly into our model without losing this advantage. Meanwhile, in mean regression, the MEM with dependencies between areas are known as the simultaneous autoregressive (SAR) model and conditional autoregressive (CAR) model (see, Rao and Molina 2015, and references therein). However, even for mean regression, the asymptotic theory for the SAR/CAR model is still to be developed. Extending our model to the SAR/CAR model and establishing its asymptotic theory are interesting future works in extreme value analysis. Of course, clustering of areas is also an important future problem for unit-level data with large area sizes (see, the references mentioned in Section 1).

Figure 18 also suggests a potential annual trend in γ_{ij} for some stations. Therefore, the observations for one year from one station can be considered as one area.

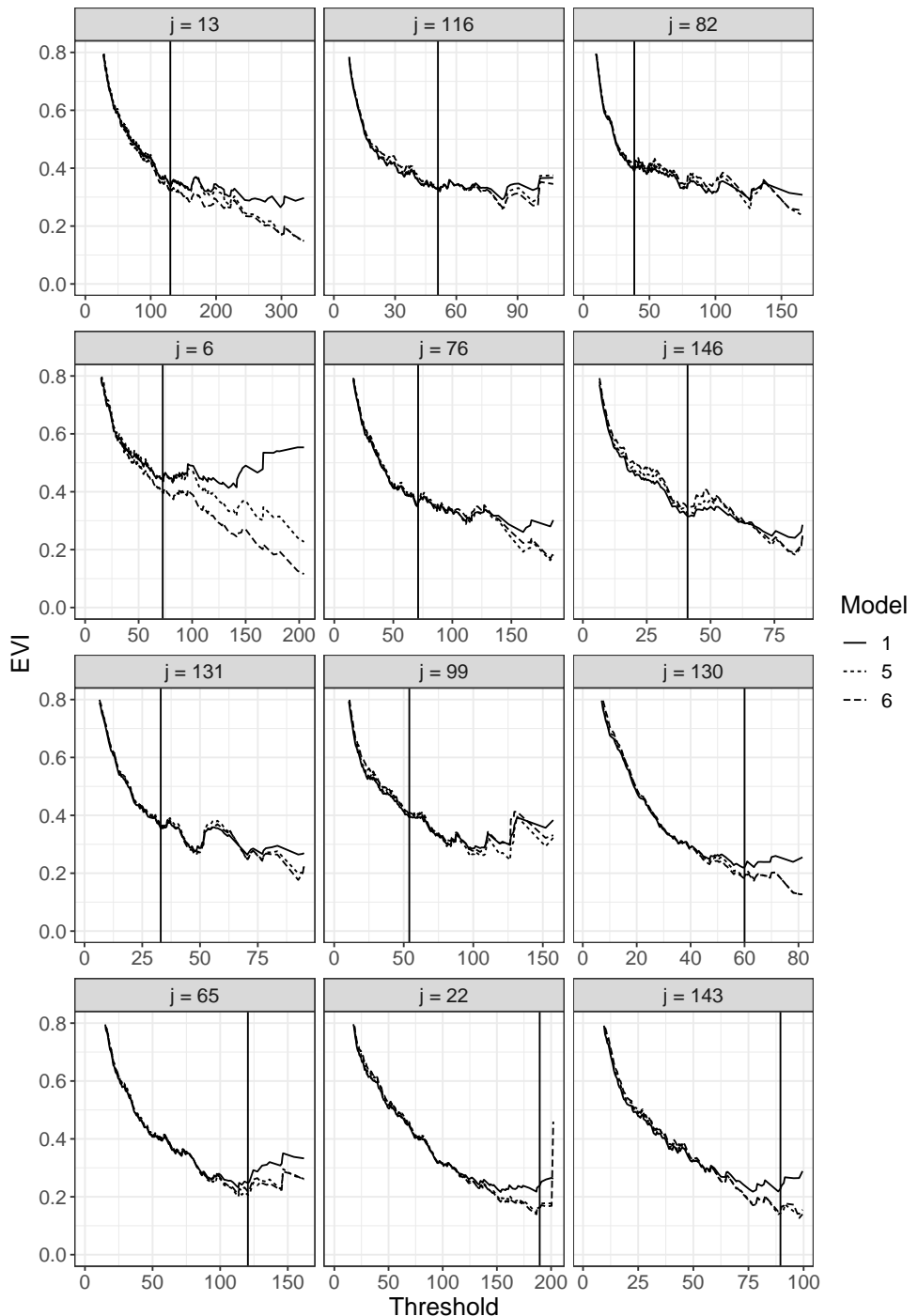


Figure 17: Plot of ω_j versus γ_j^* for $j \in \{13, 116, 82, 6, 76, 146, 131, 99, 130, 65, 22, 143\}$.

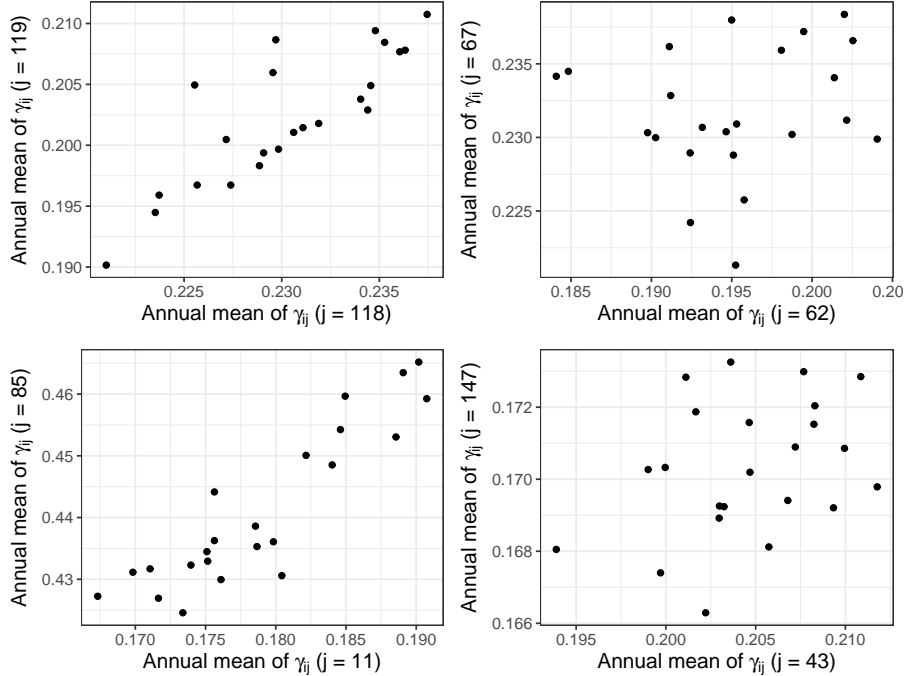


Figure 18: Plot of the annual mean of γ_{ij} for two particular stations

By extending our model to the multilevel mixed effects model with nested random effects (Ha and Lee 2005), we may more effectively analyze the differences between stations while capturing the annual trend for each station. However, because the sample size for each area becomes too small, the development of such a model with time-varying effects is posited as future work.

6 Discussion

In this study, we investigated the MEM of the EVI in the Pareto-type distribution for unit-level data. In other words, this study incorporated the method of SAE into EVT. The parameters of the proposed model were estimated by the maximum likelihood method, and the random effects were predicted by the conditional mode. We established the asymptotic normality of the estimator. Along with the simulations and real data example, we can conclude the following advantages of using the MEM for EVI regression. First, in extreme value analysis, the sample sizes of some areas are generally small because of the peak over threshold. However, in the MEM, as described in Sections 4.3 and 5, the common parametric part included in the model can adequately guide the differences between areas. Interestingly, the “borrowing of strength” of the MEM is effective for EVI regression because it improves the variance and bias of the peak over threshold method (see, Section 4.3). Thus, the proposed model provides a significantly efficient tool that is an alternative to direct estimates from each area. Second, the proposed model is effective even when the number of areas is large. This is shown theoretically in Theorem 1 of Section 3.2, while Section 4.2 proves this property numerically. Furthermore, as a result

supporting the use of the proposed model, in Sections 4.3 and 5.4, the EVT model using the MEM provided more reasonable results than the fully parametric model. Finally, in extreme value analysis, general EVI estimators sometimes have a large bias resulting from the approximation of the peak over threshold. However, from Theorem 1, we found that when J is large, the proposed estimator can be designed to reduce the bias while maintaining its stable variance. This is a somewhat surprising result, because a large number of area typically leads to poor performance of the estimator in the fully parametric model. Thus, the MEM may be one of the effective approaches to overcome the severe problem of bias in extreme value analysis.

We describe future research using the MEM for extreme value analysis. The first work of interest is developing spatial models such as SAR and CAR models to explain spatial correlations (see, Section 5.5). Such spatial work, along with spatial clustering, may help provide better estimates and easier spatial interpretation in some applications. Second, it may be feasible to extend the MEM to other EVT models such as the generalized extreme value distribution and GPD. In this study, the methods derived from these models and their theoretical results were not clarified and thus require future detailed study.

Finally, we expect to extend the MEM to extreme quantile regression (Wang et al. 2012; Wang and Li 2013).

Appendix

In this appendix, we give the proof of Theorem 1. For convenience, we introduce some symbols:

- $\boldsymbol{\theta}_C := \text{vech}(\boldsymbol{\Sigma})$, $\boldsymbol{\theta}_C^0 := \text{vech}(\boldsymbol{\Sigma}_0)$ and $\hat{\boldsymbol{\theta}}_C := \text{vech}(\hat{\boldsymbol{\Sigma}})$, which are $p_C := p_A(p_A + 1)/2$ -dimensional vectors.
- $\boldsymbol{\theta} := (\boldsymbol{\theta}_A^\top, \boldsymbol{\theta}_B^\top, \boldsymbol{\theta}_C^\top)^\top$, $\boldsymbol{\theta}^0 := ((\boldsymbol{\theta}_A^0)^\top, (\boldsymbol{\theta}_B^0)^\top, (\boldsymbol{\theta}_C^0)^\top)^\top$ and $\hat{\boldsymbol{\theta}} := (\hat{\boldsymbol{\theta}}_A^\top, \hat{\boldsymbol{\theta}}_B^\top, \hat{\boldsymbol{\theta}}_C^\top)^\top$.
- For $j \in \mathcal{J}$,

$$\ell_j(\boldsymbol{\theta}) := \log \int_{\mathbb{R}^{p_A}} \phi(\mathbf{u}; \mathbf{0}, \boldsymbol{\theta}_C) \exp \left\{ \sum_{i=1}^{n_j} \left[-(\boldsymbol{\theta}_A + \mathbf{u})^\top \mathbf{X}_{Aij} - \boldsymbol{\theta}_B^\top \mathbf{X}_{Bij} \right. \right. \\ \left. \left. - \exp \left\{ -(\boldsymbol{\theta}_A + \mathbf{u})^\top \mathbf{X}_{Aij} - \boldsymbol{\theta}_B^\top \mathbf{X}_{Bij} \right\} \log \frac{Y_{ij}}{\omega_{(J, n_j)}} \right] I(Y_{ij} > \omega_{(J, n_j)}) \right\} d\mathbf{u},$$

where $\phi(\mathbf{u}; \mathbf{0}, \boldsymbol{\theta}_C) := \phi(\mathbf{u}; \mathbf{0}, \boldsymbol{\Sigma})$. Then, the approximated log-likelihood $\ell(\boldsymbol{\theta}_A, \boldsymbol{\theta}_B, \boldsymbol{\Sigma})$ defined in (10) can be written as $\ell(\boldsymbol{\theta}) := \sum_{j=1}^J \ell_j(\boldsymbol{\theta})$.

- For any smooth function $R_1 : \mathbb{R}^d \rightarrow \mathbb{R}; \mathbf{z} \mapsto R_1(\mathbf{z})$, we denote $\nabla R_1(\mathbf{z}) := (\partial/\partial \mathbf{z}) R_1(\mathbf{z}) \in \mathbb{R}^d$ and $\nabla^2 R_1(\mathbf{z}) := (\partial^2/\partial \mathbf{z} \partial \mathbf{z}^\top) R_1(\mathbf{z}) \in \mathbb{R}^{d \times d}$. In particular, we denote $\nabla_{\mathbf{z}_0} R_1(\mathbf{z}) := (\partial/\partial \mathbf{z}_0) R_1(\mathbf{z})$ and $\nabla_{\mathbf{z}_1 \mathbf{z}_2}^2 R_1(\mathbf{z}) := (\partial^2/\partial \mathbf{z}_1 \partial \mathbf{z}_2^\top) R_1(\mathbf{z})$, where $\mathbf{z}_0, \mathbf{z}_1$ and \mathbf{z}_2 are part of \mathbf{z} . As a special case, for any smooth real-valued function $R_2(\boldsymbol{\theta})$ of $\boldsymbol{\theta} = (\boldsymbol{\theta}_A^\top, \boldsymbol{\theta}_B^\top, \boldsymbol{\theta}_C^\top)^\top$, we denote $\nabla_{\boldsymbol{\theta}_K} R_2(\boldsymbol{\theta}) := \nabla_{\boldsymbol{\theta}_K} R_2(\boldsymbol{\theta})$ and $\nabla_{\mathbf{K}_1 \mathbf{K}_2}^2 R_2(\boldsymbol{\theta}) := \nabla_{\boldsymbol{\theta}_{\mathbf{K}_1} \boldsymbol{\theta}_{\mathbf{K}_2}}^2 R_2(\boldsymbol{\theta})$ for $K, K_1, K_2 \in \{A, B, C\}$.
- For any column vector \mathbf{v} , we denote $\mathbf{v}^{\otimes 2} := \mathbf{v} \mathbf{v}^\top$.

- Let $\boldsymbol{\Upsilon}_{(J,n_0)}$ be $(p_A + p_B + p_C)$ -diagonal matrix as $\text{diag}(\boldsymbol{\Upsilon}_{(J,n_0)}) = (J^{1/2}\mathbf{1}_{p_A}^\top, J^{1/2}n_0^{1/2}\mathbf{1}_{p_B}^\top, J^{1/2}\mathbf{1}_{p_C}^\top)^\top$, where $\mathbf{1}_d$ is the d -dimensional vector with all elements 1.

Let $D_j(\mathbf{u}) := n_j P(Y_{ij} > \omega_{(J,n_j)} \mid \mathbf{U}_j = \mathbf{u})/n_0$. Then, D_j satisfies the following lemma.

Lemma 1. *Suppose that (A3) and (A4) hold. Then, under given $\mathbf{U}_j = \mathbf{u}$, $D_j(\mathbf{u}) \xrightarrow{P} d_j(\mathbf{u})$ as $n_j \rightarrow \infty$, $j \in \mathcal{J}$ and $J \rightarrow \infty$.*

Proof of Lemma 1. By straightforward calculation, we have

$$E \left[n_{j0} n_j^{-1} P(Y_{ij} > \omega_{(J,n_j)} \mid \mathbf{U}_j = \mathbf{u})^{-1} \mid \mathbf{U}_j = \mathbf{u} \right] = 1$$

and

$$\begin{aligned} & \text{var} \left[n_{j0} n_j^{-1} P(Y_{ij} > \omega_{(J,n_j)} \mid \mathbf{U}_j = \mathbf{u})^{-1} \mid \mathbf{U}_j = \mathbf{u} \right] \\ &= n_j^{-1} P(Y_{ij} > \omega_{(J,n_j)} \mid \mathbf{U}_j = \mathbf{u})^{-1} - n_j^{-1}, \end{aligned}$$

which converges to 0 as $J \rightarrow \infty$ and $n_j \rightarrow \infty$ from (A3). Therefore, under given $\mathbf{U}_j = \mathbf{u}$, as $J \rightarrow \infty$ and $n_j \rightarrow \infty$,

$$n_{j0} n_j^{-1} P(Y_{ij} > \omega_{(J,n_j)} \mid \mathbf{U}_j = \mathbf{u})^{-1} \xrightarrow{P} 1.$$

By combining this result and (A4), we obtain Lemma 1. \square

For $j \in \mathcal{J}$, we denote

$$H_j(\mathbf{u}) := n_0^{-1} \sum_{i=1}^{n_j} h_j(Y_{ij}, \mathbf{u}, \mathbf{X}_{ij}), \quad (27)$$

where

$$h_j(y, \mathbf{u}, \mathbf{x}) := \left\{ \log \gamma(\mathbf{u}, \mathbf{x}) + \gamma(\mathbf{u}, \mathbf{x})^{-1} \log \frac{y}{\omega_{(J,n_j)}} \right\} I(y > \omega_{(J,n_j)}),$$

which satisfies

$$\nabla_{\mathbf{u}} h_j(y, \mathbf{u}, \mathbf{x}) = \left\{ 1 - \gamma(\mathbf{u}, \mathbf{x})^{-1} \log \frac{y}{\omega_{(J,n_j)}} \right\} I(y > \omega_{(J,n_j)}) \mathbf{x}_A$$

and

$$\nabla_{\mathbf{u}\mathbf{u}}^2 h_j(y, \mathbf{u}, \mathbf{x}) = \gamma(\mathbf{u}, \mathbf{x})^{-1} \log \frac{y}{\omega_{(J,n_j)}} I(y > \omega_{(J,n_j)}) \mathbf{x}_A^{\otimes 2}.$$

In the following Lemmas 2 and 3, we reveal the asymptotic properties of H_j .

Lemma 2. *Suppose that (A1)-(A4) and (A6) hold. Then, under given $\mathbf{U}_j = \mathbf{u}$, as $n_j \rightarrow \infty$, $j \in \mathcal{J}$ and $J \rightarrow \infty$,*

$$n_0^{1/2} \nabla H_j(\mathbf{u}) \xrightarrow{D} N(\mathbf{0}, d_j(\mathbf{u}) \boldsymbol{\Phi}_{AA}(\mathbf{u})).$$

Proof of Lemma 2. For any $j \in \mathcal{J}$, $n_0^{1/2} \nabla H_j(\mathbf{u})$ can be written as

$$\begin{aligned} & n_0^{1/2} \nabla H_j(\mathbf{u}) \\ &= n_0^{-1/2} \sum_{i=1}^{n_j} \nabla_{\mathbf{u}} h_j(Y_{ij}, \mathbf{u}, \mathbf{X}_{ij}) \\ &= D_j(\mathbf{u})^{1/2} n_j^{-1/2} \sum_{i=1}^{n_j} \frac{\nabla_{\mathbf{u}} h_j(Y_{ij}, \mathbf{u}, \mathbf{X}_{ij}) - E[\nabla_{\mathbf{u}} h_j(Y_{ij}, \mathbf{u}, \mathbf{X}_{ij}) \mid \mathbf{U}_j = \mathbf{u}]}{P(Y_{ij} > \omega_{(J, n_j)} \mid \mathbf{U}_j = \mathbf{u})^{1/2}} \quad (28) \end{aligned}$$

$$+ D_j(\mathbf{u})^{1/2} \frac{n_j^{1/2} E[\nabla_{\mathbf{u}} h_j(Y_{ij}, \mathbf{u}, \mathbf{X}_{ij}) \mid \mathbf{U}_j = \mathbf{u}]}{P(Y_{ij} > \omega_{(J, n_j)} \mid \mathbf{U}_j = \mathbf{u})^{1/2}}. \quad (29)$$

From the following Steps 1 and 2, we obtain the asymptotic distributions of (28) and (29) conditioning $\mathbf{U}_j = \mathbf{u}$. By combining Lemma 1 and these steps, Lemma 2 holds from Slutsky's theorem.

Step 1. For (29), we show

$$\frac{J^{1/2} n_j^{1/2} E[\nabla_{\mathbf{u}} h_j(Y_{ij}, \mathbf{u}, \mathbf{X}_{ij}) \mid \mathbf{U}_j = \mathbf{u}]}{P(Y_{ij} > \omega_{(J, n_j)} \mid \mathbf{U}_j = \mathbf{u})^{1/2}} \rightarrow \mathbf{b}_{\text{Aj}}(\mathbf{u})$$

as $J \rightarrow \infty$ and $n_j \rightarrow \infty$. Since \mathbf{U}_j and \mathbf{X}_{ij} are independent of each other, we have

$$\begin{aligned} & \frac{J^{1/2} n_j^{1/2} E[\nabla_{\mathbf{u}} h_j(Y_{ij}, \mathbf{u}, \mathbf{X}_{ij}) \mid \mathbf{U}_j = \mathbf{u}]}{P(Y_{ij} > \omega_{(J, n_j)} \mid \mathbf{U}_j = \mathbf{u})^{1/2}} \\ &= \frac{J^{1/2} n_j^{1/2} E_{\mathbf{X}_{ij}} [E[\nabla_{\mathbf{u}} h_j(Y_{ij}, \mathbf{u}, \mathbf{X}_{ij}) \mid \mathbf{U}_j = \mathbf{u}, \mathbf{X}_{ij}]]}{P(Y_{ij} > \omega_{(J, n_j)} \mid \mathbf{U}_j = \mathbf{u})^{1/2}}. \quad (30) \end{aligned}$$

By the integration by parts, we have

$$\begin{aligned} & E[\nabla_{\mathbf{u}} h_j(Y_{ij}, \mathbf{u}, \mathbf{x}) \mid \mathbf{U}_j = \mathbf{u}, \mathbf{X}_{ij} = \mathbf{x}] \\ &= \left\{ \bar{F}(\omega_{(J, n_j)} \mid \mathbf{u}, \mathbf{x}) - \gamma(\mathbf{u}, \mathbf{x})^{-1} \int_0^\infty \bar{F}(\omega_{(J, n_j)} e^s \mid \mathbf{u}, \mathbf{x}) ds \right\} \mathbf{x}_{\text{A}}, \end{aligned}$$

where $\bar{F}(\cdot \mid \mathbf{u}, \mathbf{x}) := 1 - F(\cdot \mid \mathbf{u}, \mathbf{x})$. Furthermore, from (5) and (A1), we have

$$\begin{aligned} & \bar{F}(\omega_{(J, n_j)} \mid \mathbf{u}, \mathbf{x}) - \gamma(\mathbf{u}, \mathbf{x})^{-1} \int_0^\infty \bar{F}(\omega_{(J, n_j)} e^s \mid \mathbf{u}, \mathbf{x}) ds \\ &= \left\{ \frac{c_1(\mathbf{u}, \mathbf{x}) \gamma(\mathbf{u}, \mathbf{x}) \beta(\mathbf{u}, \mathbf{x})}{1 + \gamma(\mathbf{u}, \mathbf{x}) \beta(\mathbf{u}, \mathbf{x})} \omega_{(J, n_j)}^{-1/\gamma(\mathbf{u}, \mathbf{x}) - \beta(\mathbf{u}, \mathbf{x})} \right\} \{1 + o(1)\}. \end{aligned}$$

Therefore, from (A6), (30) converges to $\mathbf{b}_{\text{Aj}}(\mathbf{u})$ as $J \rightarrow \infty$ and $n_j \rightarrow \infty$.

Step 2. In this step, for (28), we show that under given $\mathbf{U}_j = \mathbf{u}$,

$$\begin{aligned} & n_j^{-1/2} \sum_{i=1}^{n_j} \frac{\nabla_{\mathbf{u}} h_j(Y_{ij}, \mathbf{u}, \mathbf{X}_{ij}) - E[\nabla_{\mathbf{u}} h_j(Y_{ij}, \mathbf{u}, \mathbf{X}_{ij}) \mid \mathbf{U}_j = \mathbf{u}]}{P(Y_{ij} > \omega_{(J, n_j)} \mid \mathbf{U}_j = \mathbf{u})^{1/2}} \\ & \xrightarrow{D} N(\mathbf{0}, \Phi_{\text{AA}}(\mathbf{u})) \quad (31) \end{aligned}$$

as $J \rightarrow \infty$ and $n_j \rightarrow \infty$. Since (31) is the sum of conditionally independent and identically distributed random vectors, we can apply the Central Limit Theorem to (31). Obviously, the conditional expectation of (31) is $\mathbf{0}$. Next, we obtain

$$\begin{aligned} & \text{cov} \left[\frac{\nabla_{\mathbf{u}} h_j(Y_{ij}, \mathbf{u}, \mathbf{X}_{ij})}{P(Y_{ij} > \omega_{(J, n_j)} \mid \mathbf{U}_j = \mathbf{u})^{1/2}} \mid \mathbf{U}_j = \mathbf{u} \right] \\ &= E \left[\frac{\nabla_{\mathbf{u}} h_j(Y_{ij}, \mathbf{u}, \mathbf{X}_{ij})^{\otimes 2}}{P(Y_{ij} > \omega_{(J, n_j)} \mid \mathbf{U}_j = \mathbf{u})} \mid \mathbf{U}_j = \mathbf{u} \right] \end{aligned} \quad (32)$$

$$- E \left[\frac{\nabla_{\mathbf{u}} h_j(Y_{ij}, \mathbf{u}, \mathbf{X}_{ij})}{P(Y_{ij} > \omega_{(J, n_j)} \mid \mathbf{U}_j = \mathbf{u})^{1/2}} \mid \mathbf{U}_j = \mathbf{u} \right]^{\otimes 2}. \quad (33)$$

From Step 1, (33) converges to \mathbf{O} as $J \rightarrow \infty$ and $n_j \rightarrow \infty$. Therefore, we show that (32) converges to $\Phi_{\text{AA}}(\mathbf{u})$ as $J \rightarrow \infty$ and $n_j \rightarrow \infty$. From (9), we have

$$\xi_j(\mathbf{u}, \mathbf{x}) := E \left[\nabla_{\mathbf{u}} h_j(Y_{ij}, \mathbf{u}, \mathbf{X}_{ij})^{\otimes 2} \mid \mathbf{U}_j = \mathbf{u}, \mathbf{X}_{ij} = \mathbf{x}, Y_{ij} > \omega_{(J, n_j)} \right] \rightarrow \mathbf{x}_{\text{A}}^{\otimes 2} \quad (34)$$

uniformly for all $\mathbf{x} \in \mathbb{R}^p$ as $J \rightarrow \infty$ and $n_j \rightarrow \infty$. In addition, from (A2), we have

$$\delta_j(\mathbf{u}, \mathbf{x}) := \frac{P(Y_{ij} > \omega_{(J, n_j)} \mid \mathbf{U}_j = \mathbf{u}, \mathbf{X}_{ij} = \mathbf{x})}{P(Y_{ij} > \omega_{(J, n_j)} \mid \mathbf{U}_j = \mathbf{u})} \rightarrow \delta(\mathbf{u}, \mathbf{x}) \quad (35)$$

uniformly for all $\mathbf{x} \in \mathbb{R}^p$ as $J \rightarrow \infty$ and $n_j \rightarrow \infty$. Now, (32) can be written as

$$E \left[\frac{\nabla_{\mathbf{u}} h_j(Y_{ij}, \mathbf{u}, \mathbf{X}_{ij})^{\otimes 2}}{P(Y_{ij} > \omega_{(J, n_j)} \mid \mathbf{U}_j = \mathbf{u})} \mid \mathbf{U}_j = \mathbf{u} \right] = E_{\mathbf{X}_{ij}} [\delta_j(\mathbf{u}, \mathbf{X}_{ij}) \xi_j(\mathbf{u}, \mathbf{X}_{ij})].$$

Therefore, from (34) and (35), (32) converges to $\Phi_{\text{AA}}(\mathbf{u})$ as $J \rightarrow \infty$ and $n_j \rightarrow \infty$. \square

Lemma 3. Suppose that (A1)-(A4) hold. Then, under given $\mathbf{U}_j = \mathbf{u}$, as $n_j \rightarrow \infty$, $j \in \mathcal{J}$ and $J \rightarrow \infty$,

$$\nabla^2 H_j(\mathbf{u}) \xrightarrow{P} d_j(\mathbf{u}) \Phi_{\text{AA}}(\mathbf{u}).$$

Proof of Lemma 3. For any $j \in \mathcal{J}$, $\nabla^2 H_j(\mathbf{u})$ can be written as

$$\begin{aligned} \nabla^2 H_j(\mathbf{u}) &= n_0^{-1} \sum_{i=1}^{n_j} \nabla_{\mathbf{u}\mathbf{u}}^2 h_j(Y_{ij}, \mathbf{u}, \mathbf{X}_{ij}) \\ &= D_j(\mathbf{u}) n_j^{-1} \sum_{i=1}^{n_j} \frac{\nabla_{\mathbf{u}\mathbf{u}}^2 h_j(Y_{ij}, \mathbf{u}, \mathbf{X}_{ij})}{P(Y_{ij} > \omega_{(J, n_j)} \mid \mathbf{U}_j = \mathbf{u})}. \end{aligned}$$

We show that under given $\mathbf{U}_j = \mathbf{u}$,

$$n_j^{-1} \sum_{i=1}^{n_j} \frac{\nabla_{\mathbf{u}\mathbf{u}}^2 h_j(Y_{ij}, \mathbf{u}, \mathbf{X}_{ij})}{P(Y_{ij} > \omega_{(J, n_j)} \mid \mathbf{U}_j = \mathbf{u})} \xrightarrow{P} \Phi_{\text{AA}}(\mathbf{u}) \quad (36)$$

as $J \rightarrow \infty$ and $n_j \rightarrow \infty$. From (9), we have

$$\boldsymbol{\xi}_j^{(1)}(\mathbf{u}, \mathbf{x}) := E \left[\nabla_{\mathbf{u}\mathbf{u}}^2 h_j(Y_{ij}, \mathbf{u}, \mathbf{x}) \mid \mathbf{U}_j = \mathbf{u}, \mathbf{X}_{ij} = \mathbf{x}, Y_{ij} > \omega_{(J, n_j)} \right] \rightarrow \mathbf{x}_A^{\otimes 2}$$

and

$$\begin{aligned} \boldsymbol{\xi}_j^{(2)}(\mathbf{u}, \mathbf{x}) &:= E \left[\text{vec} \left\{ \nabla_{\mathbf{u}\mathbf{u}}^2 h_j(Y_{ij}, \mathbf{u}, \mathbf{x}) \right\}^{\otimes 2} \mid \mathbf{U}_j = \mathbf{u}, \mathbf{X}_{ij} = \mathbf{x}, Y_{ij} > \omega_{(J, n_j)} \right] \\ &\rightarrow 2 \text{vec} \left(\mathbf{x}_A^{\otimes 2} \right)^{\otimes 2} \end{aligned}$$

uniformly for all $\mathbf{x} \in \mathbb{R}^p$ as $J \rightarrow \infty$ and $n_j \rightarrow \infty$. Now, the left-hand side of (36) has the form of the sum of conditionally independent and identically distributed random vectors, and \mathbf{U}_j and \mathbf{X}_{ij} are independent of each other. These facts yield that for (36),

$$\begin{aligned} &E \left[n_j^{-1} \sum_{i=1}^{n_j} \frac{\nabla_{\mathbf{u}\mathbf{u}}^2 h_j(Y_{ij}, \mathbf{u}, \mathbf{X}_{ij})}{P(Y_{ij} > \omega_{(J, n_j)} \mid \mathbf{U}_j = \mathbf{u})} \mid \mathbf{U}_j = \mathbf{u} \right] \\ &= E \left[\delta_j(\mathbf{u}, \mathbf{X}_{ij}) \boldsymbol{\xi}_j^{(1)}(\mathbf{u}, \mathbf{X}_{ij}) \right] \\ &\rightarrow \boldsymbol{\Phi}_{\text{AA}}(\mathbf{u}) \end{aligned}$$

and

$$\begin{aligned} &\text{cov} \left[n_j^{-1} \sum_{i=1}^{n_j} \frac{\text{vec} \left\{ \nabla_{\mathbf{u}\mathbf{u}}^2 h_j(Y_{ij}, \mathbf{u}, \mathbf{X}_{ij}) \right\}}{P(Y_{ij} > \omega_{(J, n_j)} \mid \mathbf{U}_j = \mathbf{u})} \mid \mathbf{U}_j = \mathbf{u} \right] \\ &= n_j^{-1} P(Y_{ij} > \omega_{(J, n_j)} \mid \mathbf{U}_j = \mathbf{u})^{-1} E \left[\delta_j(\mathbf{u}, \mathbf{X}_{ij}) \boldsymbol{\xi}_j^{(2)}(\mathbf{u}, \mathbf{X}_{ij}) \right] \\ &\quad - n_j^{-1} E \left[\delta_j(\mathbf{u}, \mathbf{X}_{ij}) \text{vec} \left\{ \boldsymbol{\xi}_j^{(1)}(\mathbf{u}, \mathbf{X}_{ij}) \right\} \right]^{\otimes 2} \\ &\rightarrow \mathbf{O} \end{aligned}$$

as $J \rightarrow \infty$ and $n_j \rightarrow \infty$, where δ_j is defined in (35). Therefore, (36) holds. By combining Lemma 1 and (36), we obtain Lemma 3. \square

We denote the minimizer of $H_j(\mathbf{u})$ defined in (27) as $\dot{\mathbf{U}}_j$, which satisfies the following lemma.

Lemma 4. *Suppose that (A1)-(A4) and (A6) hold. Then, as $n_j \rightarrow \infty$, $j \in \mathcal{J}$ and $J \rightarrow \infty$, $n_0^{1/2}(\dot{\mathbf{U}}_j - \mathbf{U}_j) = O_P(1)$ uniformly for all $j \in \mathcal{J}$.*

Proof of Lemma 4. We show that under given $\mathbf{U}_j = \mathbf{u}$, $n_0^{1/2}(\dot{\mathbf{U}}_j - \mathbf{u}) = O_P(1)$ uniformly for all $j \in \mathcal{J}$ and $\mathbf{u} \in \mathbb{R}^{p_A}$. By the Taylor expansion of $H_j(\mathbf{u})$, we have

$$\begin{aligned} &H_j(n_0^{-1/2} \mathbf{s} + \mathbf{u}) \\ &= H_j(\mathbf{u}) + n_0^{-1} \mathbf{s}^\top \left\{ n_0^{1/2} \nabla H_j(\mathbf{u}) \right\} + 2^{-1} n_0^{-1} \mathbf{s}^\top \nabla^2 H_j(\mathbf{u}) \mathbf{s} + o_P(1) \end{aligned}$$

for any $\mathbf{s} \in \mathbb{R}^{p_A}$ and $j \in \mathcal{J}$. From Lemmas 1 and 2, we have that for any $\varepsilon > 0$, there exists a large constant $C > 0$ such that for any $j \in \mathcal{J}$ and $\mathbf{u} \in \mathbb{R}^{p_A}$,

$$\liminf_{n_j \rightarrow \infty, j \in \mathcal{J}, J \rightarrow \infty} P \left(\inf_{\mathbf{s} \in \mathbb{R}^{p_A}: \|\mathbf{s}\|=C} H_j(n_0^{-1/2} \mathbf{s} + \mathbf{u}) > H_j(\mathbf{u}) \mid \mathbf{U}_j = \mathbf{u} \right) \geq 1 - \varepsilon. \quad (37)$$

Now, we assume that $\nabla^2 H_j(\mathbf{u})$ is the positive definite matrix for all $\mathbf{u} \in \mathbb{R}^{p_A}$, which implies that $H_j(\mathbf{u})$ is the strictly convex function. Therefore, $\dot{\mathbf{U}}_j$ is the unique global minimizer of $H_j(\mathbf{u})$. Then, we obtain Lemma 4 (the proof of Theorem 1 of Fan and Li 2001). \square

To show Lemma 6 below, we use the result of Laplace approximation, which is introduced in Lemma 5. The proof of Lemma 5 is described in (2.6) of Tierney et al. (1989), Appendix A of Miyata (2004) and (A1) of Jiang et al. (2022).

Lemma 5. *For any smooth functions g , c and $h : \mathbb{R}^d \rightarrow \mathbb{R}$,*

$$\begin{aligned} & \frac{\int g(\mathbf{u})c(\mathbf{u}) \exp\{-nh(\mathbf{u})\} d\mathbf{u}}{\int c(\mathbf{u}) \exp\{-nh(\mathbf{u})\} d\mathbf{u}} \\ &= g(\dot{\mathbf{u}}) + \frac{\nabla g(\dot{\mathbf{u}})^\top \nabla^2 h(\dot{\mathbf{u}})^{-1} \nabla c(\dot{\mathbf{u}})}{nc(\dot{\mathbf{u}})} \\ &+ \frac{\text{tr}\{\nabla^2 h(\dot{\mathbf{u}})^{-1} \nabla^2 g(\dot{\mathbf{u}})\}}{2n} - \frac{\nabla g(\dot{\mathbf{u}})^\top \nabla^2 h(\dot{\mathbf{u}})^{-1} \mathbf{a}(\dot{\mathbf{u}})}{2n} + O(n^{-2}), \end{aligned}$$

where $\dot{\mathbf{u}}$ is the minimizer of $h(\mathbf{u})$, $\mathbf{a}(\dot{\mathbf{u}})$ is the $d \times 1$ vector with the k th entry equal to $\text{tr}\{\nabla^2 h(\dot{\mathbf{u}})^{-1} \nabla^3 h(\dot{\mathbf{u}})_{[k]}\}$, $\nabla^3 h(\dot{\mathbf{u}})_{[k]}$ is the $d \times d$ matrix with the (i, j) entry equal to the (i, j, k) entry of $\nabla^3 h(\dot{\mathbf{u}})$, and $\nabla^3 h(\mathbf{u})$ denotes the $d \times d \times d$ array with the (i, j, k) entry $(\partial^3/\partial u_i \partial u_j \partial u_k)h(\mathbf{u})$.

Lemma 6. *Suppose that (A1)-(A4) and (A6) hold. Then, as $n_j \rightarrow \infty$, $j \in \mathcal{J}$ and $J \rightarrow \infty$,*

$$\nabla_{\text{A}} \ell_j(\boldsymbol{\theta}^0) = \boldsymbol{\Sigma}_0^{-1} \{ \mathbf{U}_j + n_0^{-1} d_j(\mathbf{U}_j)^{-1} \boldsymbol{\Phi}_{\text{AA}}(\mathbf{U}_j)^{-1} \mathbf{g}_{\text{A}j}(\mathbf{U}_j) \} + O_P(n_0^{-1}), \quad (38)$$

$$\nabla_{\text{B}} \ell_j(\boldsymbol{\theta}^0) = \mathbf{g}_{\text{B}j}(\mathbf{U}_j) - \boldsymbol{\Phi}_{\text{AB}}(\mathbf{U}_j)^\top \boldsymbol{\Phi}_{\text{AA}}(\mathbf{U}_j)^{-1} \mathbf{g}_{\text{A}j}(\mathbf{U}_j) + O_P(1) \quad (39)$$

and

$$\begin{aligned} \nabla_{\text{C}} \ell_j(\boldsymbol{\theta}^0) &= 2^{-1} \mathbf{M}_* (\boldsymbol{\Sigma}_0 \otimes \boldsymbol{\Sigma}_0)^{-1} \\ &\times \text{vec} \left\{ \mathbf{U}_j^{\otimes 2} - \boldsymbol{\Sigma}_0 + n_0^{-1} d_j(\mathbf{U}_j)^{-1} \mathbf{U}_j \mathbf{g}_{\text{A}j}(\mathbf{U}_j)^\top \boldsymbol{\Phi}_{\text{AA}}(\mathbf{U}_j)^{-1} \right. \\ &\left. + n_0^{-1} d_j(\mathbf{U}_j)^{-1} \boldsymbol{\Phi}_{\text{AA}}(\mathbf{U}_j)^{-1} \mathbf{g}_{\text{A}j}(\mathbf{U}_j) \mathbf{U}_j^\top \right\} + O_P(n_0^{-1}), \end{aligned} \quad (40)$$

where

$$\mathbf{g}_{\text{K}j}(\mathbf{u}) := \sum_{i=1}^{n_j} \left\{ \gamma(\mathbf{u}, \mathbf{X}_{ij})^{-1} \log \frac{Y_{ij}}{\omega_{(J, n_j)}} - 1 \right\} I(Y_{ij} > \omega_{(J, n_j)}) \mathbf{X}_{\text{K}ij}$$

for $j \in \mathcal{J}$ and $\text{K} \in \{\text{A}, \text{B}\}$.

Proof of Lemma 6. For any $j \in \mathcal{J}$, $\nabla_{\text{K}} \ell_j(\boldsymbol{\theta}^0)$, $\text{K} \in \{\text{A}, \text{B}, \text{C}\}$ can be written as

$$\begin{aligned} \nabla_{\text{A}} \ell_j(\boldsymbol{\theta}^0) &= \frac{\int_{\mathbb{R}^{p_A}} \mathbf{g}_{\text{A}j}(\mathbf{u}) c_D(\mathbf{u}) \exp\{-n_0 H_j(\mathbf{u})\} d\mathbf{u}}{\int_{\mathbb{R}^{p_A}} c_D(\mathbf{u}) \exp\{-n_0 H_j(\mathbf{u})\} d\mathbf{u}}, \\ \nabla_{\text{B}} \ell_j(\boldsymbol{\theta}^0) &= \frac{\int_{\mathbb{R}^{p_A}} \mathbf{g}_{\text{B}j}(\mathbf{u}) c_D(\mathbf{u}) \exp\{-n_0 H_j(\mathbf{u})\} d\mathbf{u}}{\int_{\mathbb{R}^{p_A}} c_D(\mathbf{u}) \exp\{-n_0 H_j(\mathbf{u})\} d\mathbf{u}} \end{aligned}$$

and

$$\nabla_C \ell_j(\boldsymbol{\theta}^0) = \frac{\int_{\mathbb{R}^{p_A}} \mathbf{g}_{Cj}(\mathbf{u}) c_D(\mathbf{u}) \exp \{-n_0 H_j(\mathbf{u})\} d\mathbf{u}}{\int_{\mathbb{R}^{p_A}} c_D(\mathbf{u}) \exp \{-n_0 H_j(\mathbf{u})\} d\mathbf{u}} - 2^{-1} \mathbf{M}_* \text{vec}(\boldsymbol{\Sigma}_0^{-1}),$$

where $c_D(\mathbf{u}) := \exp(-2^{-1} \mathbf{u}^\top \boldsymbol{\Sigma}_0^{-1} \mathbf{u})$ and $\mathbf{g}_{Cj}(\mathbf{u}) := 2^{-1} \mathbf{M}_* (\boldsymbol{\Sigma}_0 \otimes \boldsymbol{\Sigma}_0)^{-1} \text{vec}(\mathbf{u}^{\otimes 2})$. For each $l \in \{1, 2, \dots, p_K\}$, we denote the l th component of \mathbf{g}_{Kj} as $g_{Kj}^{(l)}$. From Lemma 5, we then have

$$\begin{aligned} & \frac{\int_{\mathbb{R}^{p_A}} \mathbf{g}_{Kj}(\mathbf{u}) c_D(\mathbf{u}) \exp \{-n_0 H_j(\mathbf{u})\} d\mathbf{u}}{\int_{\mathbb{R}^{p_A}} c_D(\mathbf{u}) \exp \{-n_0 H_j(\mathbf{u})\} d\mathbf{u}} \\ &= \mathbf{g}_{Kj}(\dot{\mathbf{U}}_j) + \left[\frac{\nabla g_{Kj}^{(l)}(\dot{\mathbf{U}}_j)^\top \nabla^2 H_j(\dot{\mathbf{U}}_j)^{-1} \nabla c_D(\dot{\mathbf{U}}_j)}{n_0 c_D(\dot{\mathbf{U}}_j)} \right]_{p_K \times 1, 1 \leq l \leq p_K} \\ &+ \left[\frac{\text{tr} \left\{ \nabla^2 H_j(\dot{\mathbf{U}}_j)^{-1} \nabla^2 g_{Kj}^{(l)}(\dot{\mathbf{U}}_j) \right\}}{2n_0} \right]_{p_K \times 1, 1 \leq l \leq p_K} \\ &- \left[\frac{\nabla g_{Kj}^{(l)}(\dot{\mathbf{U}}_j)^\top \nabla^2 H_j(\dot{\mathbf{U}}_j)^{-1} \mathbf{a}_j(\dot{\mathbf{U}}_j)}{2n_0} \right]_{p_K \times 1, 1 \leq l \leq p_K} + O(n_0^{-2}) \end{aligned} \quad (41)$$

for $j \in \mathcal{J}$ and $K \in \{A, B, C\}$. In the following Steps 1-3, we evaluate $\nabla_K \ell_j(\boldsymbol{\theta}^0)$ based on (41).

Step 1. We apply (41) to $\nabla_A \ell_j(\boldsymbol{\theta}^0)$. By straightforward calculation, we have $\mathbf{g}_{Aj}(\dot{\mathbf{U}}_j) = \mathbf{0}$,

$$\left[\frac{\nabla g_{Aj}^{(l)}(\dot{\mathbf{U}}_j)^\top \nabla^2 H_j(\dot{\mathbf{U}}_j)^{-1} \nabla c_D(\dot{\mathbf{U}}_j)}{n_0 c_D(\dot{\mathbf{U}}_j)} \right]_{p_A \times 1, 1 \leq l \leq p_A} = \boldsymbol{\Sigma}_0^{-1} \dot{\mathbf{U}}_j$$

and

$$\frac{\text{tr} \left\{ \nabla^2 H_j(\dot{\mathbf{U}}_j)^{-1} \nabla^2 g_{Aj}^{(l)}(\dot{\mathbf{U}}_j) \right\}}{2n_0} - \frac{\nabla g_{Aj}^{(l)}(\dot{\mathbf{U}}_j)^\top \nabla^2 H_j(\dot{\mathbf{U}}_j)^{-1} \mathbf{a}_j(\dot{\mathbf{U}}_j)}{2n_0} = 0$$

for $l \in \{1, 2, \dots, p_A\}$. Furthermore, from Lemmas 3 and 4, by the Taylor expansion of $\nabla H_j(\mathbf{u})$, we obtain

$$\dot{\mathbf{U}}_j = \mathbf{U}_j + n_0^{-1} d_j(\mathbf{U}_j)^{-1} \boldsymbol{\Phi}_{AA}(\mathbf{U}_j)^{-1} \mathbf{g}_{Aj}(\mathbf{U}_j) + O_P(n_0^{-1}). \quad (42)$$

Consequently, we obtain (38).

Step 2. In this step, (41) is applied to $\nabla_B \ell_j(\boldsymbol{\theta}^0)$. From Lemma 4, by the Taylor expansion of $\mathbf{g}_{Bj}(\mathbf{u})$, (42) and the similar results to Lemma 3, we obtain

$$\begin{aligned} \mathbf{g}_{Bj}(\dot{\mathbf{U}}_j) &= \mathbf{g}_{Bj}(\mathbf{U}_j) - n_0 d_j(\mathbf{U}_j) \boldsymbol{\Phi}_{AB}(\mathbf{U}_j)^\top (\dot{\mathbf{U}}_j - \mathbf{U}_j) \{1 + o_P(1)\} \\ &= \mathbf{g}_{Bj}(\mathbf{U}_j) - \boldsymbol{\Phi}_{AB}(\mathbf{U}_j)^\top \boldsymbol{\Phi}_{AA}(\mathbf{U}_j)^{-1} \mathbf{g}_{Aj}(\mathbf{U}_j) + O_P(1). \end{aligned}$$

In addition, we have

$$\begin{aligned} & \frac{\nabla g_{Bj}^{(l)}(\dot{\mathbf{U}}_j)^\top \nabla^2 H_j(\dot{\mathbf{U}}_j)^{-1} \nabla c_D(\dot{\mathbf{U}}_j)}{n_0 c_D(\dot{\mathbf{U}}_j)} + \frac{\text{tr} \left\{ \nabla^2 H_j(\dot{\mathbf{U}}_j)^{-1} \nabla^2 g_{Bj}^{(l)}(\dot{\mathbf{U}}_j) \right\}}{2n_0} \\ & - \frac{\nabla g_{Bj}^{(l)}(\dot{\mathbf{U}}_j)^\top \nabla^2 H_j(\dot{\mathbf{U}}_j)^{-1} \mathbf{a}_j(\dot{\mathbf{U}}_j)}{2n_0} = O_P(1) \end{aligned}$$

for $l \in \{1, 2, \dots, p_B\}$. Consequently, (39) is obtained.

Step 3. In the last step, we calculate $\nabla_C \ell_j(\boldsymbol{\theta}^0)$ along with (41). From (42), we have

$$\begin{aligned} \mathbf{g}_{Cj}(\dot{\mathbf{U}}_j) &= 2^{-1} \mathbf{M}_* (\boldsymbol{\Sigma}_0 \otimes \boldsymbol{\Sigma}_0)^{-1} \text{vec} \left(\dot{\mathbf{U}}_j^{\otimes 2} \right) \\ &= 2^{-1} \mathbf{M}_* (\boldsymbol{\Sigma}_0 \otimes \boldsymbol{\Sigma}_0)^{-1} \\ &\quad \times \text{vec} \left\{ \dot{\mathbf{U}}_j^{\otimes 2} + n_0^{-1} d_j(\mathbf{U}_j)^{-1} \mathbf{U}_j \mathbf{g}_{Aj}(\mathbf{U}_j)^\top \boldsymbol{\Phi}_{AA}(\mathbf{U}_j)^{-1} \right. \\ &\quad \left. + n_0^{-1} d_j(\mathbf{U}_j)^{-1} \boldsymbol{\Phi}_{AA}(\mathbf{U}_j)^{-1} \mathbf{g}_{Aj}(\mathbf{U}_j) \mathbf{U}_j^\top \right\} + O_P(n_0^{-1}). \end{aligned}$$

Additionally, we have

$$\begin{aligned} & \frac{\nabla g_{Cj}^{(l)}(\dot{\mathbf{U}}_j)^\top \nabla^2 H_j(\dot{\mathbf{U}}_j)^{-1} \nabla c_D(\dot{\mathbf{U}}_j)}{n_0 c_D(\dot{\mathbf{U}}_j)} + \frac{\text{tr} \left\{ \nabla^2 H_j(\dot{\mathbf{U}}_j)^{-1} \nabla^2 g_{Cj}^{(l)}(\dot{\mathbf{U}}_j) \right\}}{2n_0} \\ & - \frac{\nabla g_{Cj}^{(l)}(\dot{\mathbf{U}}_j)^\top \nabla^2 H_j(\dot{\mathbf{U}}_j)^{-1} \mathbf{a}_j(\dot{\mathbf{U}}_j)}{2n_0} = O_P(n_0^{-1}) \end{aligned}$$

for $l \in \{1, 2, \dots, p_C\}$. Thus, (40) is shown. \square

Lemma 6 leads to the following Lemmas 7-9.

Lemma 7. *Suppose that (A1)-(A6) hold. Then, as $n_j \rightarrow \infty$, $j \in \mathcal{J}$ and $J \rightarrow \infty$,*

$$J^{-1/2} \nabla_A \ell(\boldsymbol{\theta}^0) + n_0^{-1/2} \boldsymbol{\Delta}_A^{-1} \mathbf{b}_A \xrightarrow{D} N(\mathbf{0}, \boldsymbol{\Delta}_A^{-1}).$$

Proof of Lemma 7. Let

$$\mathbf{Z} := J^{-1/2} \sum_{j=1}^J n_0^{-1/2} d_j(\mathbf{U}_j)^{-1} \boldsymbol{\Phi}_{AA}(\mathbf{U}_j)^{-1} \mathbf{g}_{Aj}(\mathbf{U}_j).$$

From Lemma 6, we then have

$$J^{-1/2} \nabla_A \ell(\boldsymbol{\theta}^0) = J^{-1/2} \sum_{j=1}^J \boldsymbol{\Sigma}_0^{-1} \mathbf{U}_j + n_0^{-1/2} \boldsymbol{\Sigma}_0^{-1} \mathbf{Z} \{1 + o_P(1)\}. \quad (43)$$

From the reproductive property of the normal distribution, the first term on the right-hand side of (43) converges to $N(\mathbf{0}, \boldsymbol{\Sigma}_0^{-1})$ in distribution as $J \rightarrow \infty$. From the

proof of Lemma 2, for the second term of the right-hand side of (43), we have

$$\begin{aligned}
E[\mathbf{Z}] &= J^{-1} \sum_{j=1}^J E \left[d_j(\mathbf{U}_j)^{-1} \Phi_{AA}(\mathbf{U}_j)^{-1} E \left[J^{1/2} n_0^{-1/2} \mathbf{g}_{Aj}(\mathbf{U}_j) \mid \mathbf{U}_j \right] \right] \\
&= - \left\{ J^{-1} \sum_{j=1}^J E \left[d_j(\mathbf{U}_j)^{-1/2} \Phi_{AA}(\mathbf{U}_j)^{-1} \mathbf{b}_{Aj}(\mathbf{U}_j) \right] \right\} \{1 + o(1)\} \\
&= -\mathbf{b}_A \{1 + o(1)\}
\end{aligned}$$

and $\text{cov}[n_0^{-1/2} \mathbf{Z}] \rightarrow \mathbf{O}$, which implies that the sum of $n_0^{-1/2} \Sigma_0^{-1} \mathbf{b}_A$ and the second term on the right-hand side of (43) converges to $\mathbf{0}$ in probability as $n_j \rightarrow \infty$, $j \in \mathcal{J}$ and $J \rightarrow \infty$. Thus, Lemma 7 is shown. \square

Lemma 8. Suppose that (A1)-(A6) hold. Then, as $n_j \rightarrow \infty$, $j \in \mathcal{J}$ and $J \rightarrow \infty$,

$$J^{-1/2} n_0^{-1/2} \nabla_B \ell(\boldsymbol{\theta}^0) \xrightarrow{D} N(-\Delta_B^{-1} \mathbf{b}_B, \Delta_B^{-1}).$$

Proof of Lemma 8. We denote

$$\mathbf{W}_j(\mathbf{u}) := \mathbf{g}_{Bj}(\mathbf{u}) - \Phi_{AB}(\mathbf{u})^\top \Phi_{AA}(\mathbf{u})^{-1} \mathbf{g}_{Aj}(\mathbf{u}).$$

From Lemma 6, we have

$$J^{-1/2} n_0^{-1/2} \nabla_B \ell(\boldsymbol{\theta}^0) = \left\{ J^{-1/2} \sum_{j=1}^J n_0^{-1/2} \mathbf{W}_j(\mathbf{U}_j) \right\} \{1 + o_P(1)\}. \quad (44)$$

Now, the right-hand side of (44) can be written as

$$\begin{aligned}
&J^{-1/2} \sum_{j=1}^J n_0^{-1/2} \mathbf{W}_j(\mathbf{U}_j) \\
&= J^{-1/2} \sum_{j=1}^J n_{j0}^{1/2} n_0^{-1/2} \left\{ n_{j0}^{-1/2} \mathbf{W}_j(\mathbf{U}_j) - E \left[n_{j0}^{-1/2} \mathbf{W}_j(\mathbf{U}_j) \mid \mathbf{U}_j \right] \right\} \quad (45) \\
&\quad + J^{-1} \sum_{j=1}^J E \left[J^{1/2} n_0^{-1/2} \mathbf{W}_j(\mathbf{U}_j) \mid \mathbf{U}_j \right].
\end{aligned}$$

Similar to the proof of Lemma 7, (46) converges to $-\Delta_B^{-1} \mathbf{b}_B$ in probability as $n_j \rightarrow \infty$, $j \in \mathcal{J}$ and $J \rightarrow \infty$. Similar to Lemma 2, for (45), we have that under given $\mathbf{U}_j = \mathbf{u}_j$,

$$\begin{aligned}
&n_{j0}^{-1/2} \mathbf{W}_j(\mathbf{u}_j) - E \left[n_{j0}^{-1/2} \mathbf{W}_j(\mathbf{u}_j) \mid \mathbf{U}_j = \mathbf{u}_j \right] \\
&\xrightarrow{D} N(\mathbf{0}, \Phi_{BB}(\mathbf{u}_j) - \Phi_{AB}(\mathbf{u}_j)^\top \Phi_{AA}(\mathbf{u}_j)^{-1} \Phi_{AB}(\mathbf{u}_j))
\end{aligned}$$

as $J \rightarrow \infty$ and $n_j \rightarrow \infty$. Therefore, (45) is the weighted sum of independent and asymptotically identically distributed random vectors, which can be applied the weighted central limit theorem (Weber 2006). As a result, (45) converges to $N(\mathbf{0}, \Delta_B^{-1})$ in distribution as $n_j \rightarrow \infty$, $j \in \mathcal{J}$ and $J \rightarrow \infty$. Thus, the proof of Lemma 8 is completed. \square

Lemma 9. Suppose that (A1)-(A6) hold. Then, as $n_j \rightarrow \infty$, $j \in \mathcal{J}$ and $J \rightarrow \infty$,

$$J^{-1/2} \nabla_C \ell(\boldsymbol{\theta}^0) + n_0^{-1/2} \boldsymbol{\Delta}_C^{-1} \mathbf{b}_C \xrightarrow{D} N(\mathbf{0}, \boldsymbol{\Delta}_C^{-1}).$$

Proof of Lemma 9. Let

$$\mathbf{V}_j(\mathbf{u}) := d_j(\mathbf{u})^{-1} \left\{ \mathbf{u} \mathbf{g}_{Aj}(\mathbf{u})^\top \boldsymbol{\Phi}_{AA}(\mathbf{u})^{-1} + \boldsymbol{\Phi}_{AA}(\mathbf{u})^{-1} \mathbf{g}_{Aj}(\mathbf{u}) \mathbf{u}^\top \right\}.$$

From Lemma 6, we obtain

$$\begin{aligned} & J^{-1/2} \nabla_C \ell(\boldsymbol{\theta}^0) \\ &= 2^{-1} \mathbf{M}_* (\boldsymbol{\Sigma}_0 \otimes \boldsymbol{\Sigma}_0)^{-1} J^{-1/2} \sum_{j=1}^J \text{vec} \left(\mathbf{U}_j^{\otimes 2} - \boldsymbol{\Sigma}_0 \right) \end{aligned} \quad (47)$$

$$+ 2^{-1} \mathbf{M}_* (\boldsymbol{\Sigma}_0 \otimes \boldsymbol{\Sigma}_0)^{-1} n_0^{-1/2} \left[J^{-1/2} \sum_{j=1}^J n_0^{-1/2} \text{vec} \{ \mathbf{V}_j(\mathbf{U}_j) \} \right] \{1 + o_P(1)\}. \quad (48)$$

$\mathbf{U}_j^{\otimes 2}$ is distributed as a Wishart distribution with $E[\mathbf{U}_j^{\otimes 2}] = \boldsymbol{\Sigma}_0$ and $\text{cov}[\text{vec}(\mathbf{U}_j^{\otimes 2})] = 2(\boldsymbol{\Sigma}_0 \otimes \boldsymbol{\Sigma}_0)$. Therefore, by the Central Limit Theorem, (47) converges to $N(\mathbf{0}, \boldsymbol{\Delta}_C^{-1})$ in distribution as $J \rightarrow \infty$. Moreover, similar to the proof of Lemma 7, (48) is asymptotically equivalent to $-n_0^{-1/2} \boldsymbol{\Delta}_C^{-1} \mathbf{b}_C$, which completes the proof of Lemma 9. \square

The above Lemmas 7-9 are summarized following two propositions.

Proposition 1. Suppose that (A1)-(A6) hold. Then, as $n_j \rightarrow \infty$, $j \in \mathcal{J}$ and $J \rightarrow \infty$,

$$\boldsymbol{\Upsilon}_{(J,n_0)}^{-1} \nabla \ell(\boldsymbol{\theta}^0) + \begin{bmatrix} n_0^{-1/2} \boldsymbol{\Delta}_A^{-1} \mathbf{b}_A \\ \boldsymbol{\Delta}_B^{-1} \mathbf{b}_B \\ n_0^{-1/2} \boldsymbol{\Delta}_C^{-1} \mathbf{b}_C \end{bmatrix} \xrightarrow{D} N \left(\mathbf{0}, \begin{bmatrix} \boldsymbol{\Delta}_A^{-1} & \mathbf{O} & \mathbf{O} \\ \mathbf{O} & \boldsymbol{\Delta}_B^{-1} & \mathbf{O} \\ \mathbf{O} & \mathbf{O} & \boldsymbol{\Delta}_C^{-1} \end{bmatrix} \right).$$

Proof of Proposition 1. Similar to Lemmas 7-9, from Lemma 6, we have

$$\begin{aligned} & \text{cov} \left[J^{-1/2} \nabla_A \ell(\boldsymbol{\theta}^0), J^{-1/2} n_0^{-1/2} \nabla_B \ell(\boldsymbol{\theta}^0) \right] \rightarrow \mathbf{O}, \\ & \text{cov} \left[J^{-1/2} \nabla_A \ell(\boldsymbol{\theta}^0), J^{-1/2} \nabla_C \ell(\boldsymbol{\theta}^0) \right] \rightarrow \mathbf{O} \end{aligned}$$

and

$$\text{cov} \left[J^{-1/2} n_0^{-1/2} \nabla_B \ell(\boldsymbol{\theta}^0), J^{-1/2} \nabla_C \ell(\boldsymbol{\theta}^0) \right] \rightarrow \mathbf{O}$$

as $n_j \rightarrow \infty$, $j \in \mathcal{J}$ and $J \rightarrow \infty$. Combining these results and Lemmas 7-9, we obtain Proposition 1. \square

Proposition 2. Suppose that (A1)-(A6) hold. Then, as $n_j \rightarrow \infty$, $j \in \mathcal{J}$ and $J \rightarrow \infty$,

$$\boldsymbol{\Upsilon}_{(J,n_0)}^{-1} \nabla^2 \ell(\boldsymbol{\theta}^0) \boldsymbol{\Upsilon}_{(J,n_0)}^{-1} \xrightarrow{P} \begin{bmatrix} -\boldsymbol{\Delta}_A^{-1} & \mathbf{O} & \mathbf{O} \\ \mathbf{O} & -\boldsymbol{\Delta}_B^{-1} & \mathbf{O} \\ \mathbf{O} & \mathbf{O} & -\boldsymbol{\Delta}_C^{-1} \end{bmatrix}.$$

Proof of Proposition 2. From Lemma 5 of Nie (2007) and Lemma 5, the covariance matrix of $\text{vec}(\mathbf{\Upsilon}_{(J,n_0)}^{-1} \nabla^2 \ell(\boldsymbol{\theta}^0) \mathbf{\Upsilon}_{(J,n_0)}^{-1})$ converges to \mathbf{O} as $n_j \rightarrow \infty$, $j \in \mathcal{J}$ and $J \rightarrow \infty$. Now, we have

$$E \left[\mathbf{\Upsilon}_{(J,n_0)}^{-1} \nabla^2 \ell(\boldsymbol{\theta}^0) \mathbf{\Upsilon}_{(J,n_0)}^{-1} \right] = -E \left[\mathbf{\Upsilon}_{(J,n_0)}^{-1} \nabla \ell(\boldsymbol{\theta}^0)^{\otimes 2} \mathbf{\Upsilon}_{(J,n_0)}^{-1} \right]. \quad (49)$$

By calculating the right-hand side of (49) using Lemma 6, Proposition 2 is obtained. \square

Proof of Theorem 1. For any $\boldsymbol{\theta} \in \mathbb{R}^{p_A + p_B + p_C}$, the Taylor expansion of $\ell(\boldsymbol{\theta})$ around $\boldsymbol{\theta} = \boldsymbol{\theta}^0$ yields that

$$\begin{aligned} & \ell(\mathbf{\Upsilon}_{(J,n_0)}^{-1} \boldsymbol{\theta} + \boldsymbol{\theta}^0) \\ &= \ell(\boldsymbol{\theta}^0) + \boldsymbol{\theta}^\top \mathbf{\Upsilon}_{(J,n_0)}^{-1} \nabla \ell(\boldsymbol{\theta}^0) + 2^{-1} \boldsymbol{\theta}^\top \mathbf{\Upsilon}_{(J,n_0)}^{-1} \nabla^2 \ell(\boldsymbol{\theta}^0) \mathbf{\Upsilon}_{(J,n_0)}^{-1} \boldsymbol{\theta} + o_P(1). \end{aligned}$$

From Propositions 1 and 2, for any $\varepsilon > 0$, there exists a large constant $C > 0$ such that

$$\liminf_{n_j \rightarrow \infty, j \in \mathcal{J}, J \rightarrow \infty} P \left(\inf_{\boldsymbol{\theta} \in \mathbb{R}^{p_A + p_B + p_C}: \|\boldsymbol{\theta}\| = C} -\ell(\mathbf{\Upsilon}_{(J,n_0)}^{-1} \boldsymbol{\theta} + \boldsymbol{\theta}^0) > -\ell(\boldsymbol{\theta}^0) \right) \geq 1 - \varepsilon \quad (50)$$

as $n_j \rightarrow \infty$, $j \in \mathcal{J}$ and $J \rightarrow \infty$. We assume that $-\nabla^2 \ell(\boldsymbol{\theta})$ is the positive definite matrix for all $\boldsymbol{\theta}$, which implies that $-\ell(\boldsymbol{\theta})$ is the strictly convex function. Therefore, $\hat{\boldsymbol{\theta}}$ is the unique global maximizer of $\ell(\boldsymbol{\theta})$. Then, (50) implies $\mathbf{\Upsilon}_{(J,n_0)}(\hat{\boldsymbol{\theta}} - \boldsymbol{\theta}^0) = O_P(1)$ (the proof of Theorem 1 of Fan and Li 2001). Since $\hat{\boldsymbol{\theta}}$ is the global maximizer of $\ell(\boldsymbol{\theta})$, we have $\nabla \ell(\hat{\boldsymbol{\theta}}) = \mathbf{0}$. From the Taylor expansion of $\ell(\boldsymbol{\theta})$, we have

$$\mathbf{\Upsilon}_{(J,n_0)}(\hat{\boldsymbol{\theta}} - \boldsymbol{\theta}^0) = -\left\{ \mathbf{\Upsilon}_{(J,n_0)}^{-1} \nabla^2 \ell(\boldsymbol{\theta}^0) \mathbf{\Upsilon}_{(J,n_0)}^{-1} \right\}^{-1} \mathbf{\Upsilon}_{(J,n_0)}^{-1} \nabla \ell(\boldsymbol{\theta}^0) + o_P(1).$$

Therefore, by applying Propositions 1 and 2, we obtain Theorem 1. \square

References

- [1] Almeida, S., Loy, A., Hofmann, H.: ggplot2 Compatible Quantile-Quantile Plots in R. The R Journal **10**(2), 248-261 (2018). <https://doi.org/10.32614/RJ-2018-051>
- [2] Bandaru, S., Sano, S., Shimizu, Y., Seki, Y., Okano, Y., Sasaki, T., Wada, H., Otsuki, T., Ito, T.: Impact of heavy rains of 2018 in western Japan: disaster-induced health outcomes among the population of Innoshima Island. Heliyon **6**(5), e03942 (2020). <https://doi.org/10.1016/j.heliyon.2020.e03942>
- [3] Bates, D., Mächler, M., Bolker, B., Walker, S.: Fitting Linear Mixed-Effects Models Using lme4. Journal of Statistical Software **67**(1), 1-48 (2015). <https://doi.org/10.18637/jss.v067.i01>
- [4] Battese, G., Harter, R., Fuller, W.: An Error-Components Model for Prediction of County Crop Areas Using Survey and Satellite Data. Journal of the American Statistical Association **83**(401), 28-36 (1988). <https://doi.org/10.1080/01621459.1988.10478561>

[5] Beirlant, J., Goegebeur, Y.: Regression with response distributions of Pareto-type. *Computational Statistics & Data Analysis* **42**(4), 595-619 (2003). [https://doi.org/10.1016/S0167-9473\(02\)00120-2](https://doi.org/10.1016/S0167-9473(02)00120-2)

[6] Beirlant, J., Goegebeur, Y., Teugels, J., Segers, J.: *Statistics of Extremes: Theory and Applications*. Wiley Series in Probability and Statistics. John Wiley & Sons, New Jersey (2004). <https://doi.org/10.1002/0470012382>

[7] Bottolo, L., Consonni, G., Dellaportas, P., Lijoi, A.: Bayesian Analysis of Extreme Values by Mixture Modeling. *Extremes* **6**(1), 25-47 (2003). <https://doi.org/10.1023/A:1026225113154>

[8] Broström, G., Holmberg, H.: Generalized linear models with clustered data: Fixed and random effects models. *Computational Statistics & Data Analysis* **55**(12), 3123-3134 (2011). <https://doi.org/10.1016/j.csda.2011.06.011>

[9] Davison, A. C., Smith, R. L.: Models for Exceedances Over High Thresholds. *Journal of the Royal Statistical Society: Series B (Methodological)* **52**(3), 393-425 (1990). <https://doi.org/10.1111/j.2517-6161.1990.tb01796.x>

[10] de Carvalho, M., Huser, R., Rubio, R.: Similarity-based clustering for patterns of extreme values. *Stat* **12**(1), e560 (2023). <https://onlinelibrary.wiley.com/doi/abs/10.1002/sta4.560>

[11] Dempster, A. P., Rubin, D. B., Tsutakawa, R. K.: Estimation in Covariance Components Models. *Journal of the American Statistical Association* **76**(374), 341-353 (1981). <https://www.tandfonline.com/doi/abs/10.1080/01621459.1981.10477653>

[12] Diallo, M., Rao, J.N.K.: Small area estimation of complex parameters under unit-level models with skew-normal errors. *Scandinavian Journal of Statistics* **45**(4), 1092-1116 (2018). <https://doi.org/10.1111/sjos.12336>

[13] Dupuis, D. J., Engelke, S., Trapin, L.: Modeling panels of extremes. *The Annals of Applied Statistics* **17**(1), 498-517 (2023). <https://doi.org/10.1214/22-AOAS1639>

[14] Einmahl, J. J., and Einmahl, J. H. J., de Haan, L.: Limits to Human Life Span Through Extreme Value Theory. *Journal of the American Statistical Association* **114**(527), 1075-1080 (2019). <https://doi.org/10.1080/01621459.2018.1537912>

[15] Fan, J., Li, R.: Variable Selection via Nonconcave Penalized Likelihood and its Oracle Properties. *Journal of the American Statistical Association* **96**(456), 1348-1360 (2001). <https://doi.org/10.1198/016214501753382273>

[16] Fisher, R., Tippett, L.: Limiting forms of the frequency distribution of the largest or smallest member of a sample. *Mathematical Proceedings of the Cambridge Philosophical Society* **24**(2), 180-190 (1928). <https://doi.org/10.1017/S0305004100015681>

[17] Gumbel, E. J.: *Statistics of Extremes*. Columbia University Press, West Sussex (1958). <https://doi.org/10.7312/gumb92958>

[18] Ha, I. D., Lee, Y.: Multilevel mixed linear models for survival data. *Lifetime Data Analysis* **11**(1), 131-142 (2005). <https://doi.org/10.1007/s10985-004-5644-2>

[19] Hall, P.: On Some Simple Estimates of an Exponent of Regular Variation. *Journal of the Royal Statistical Society: Series B (Methodological)* **44**(1), 37-42 (1982). <https://doi.org/10.1111/j.2517-6161.1982.tb01183.x>

[20] Hill, B. M.: A Simple General Approach to Inference About the Tail of a Distribution. *The Annals of Statistics* **3**(5), 1163-1174 (1975). <https://doi.org/10.1214/aos/1176343247>

[21] Jiang, J.: Linear and Generalized Linear Mixed Models and Their Applications. Springer Series in Statistics. Springer, New York (2007). <https://doi.org/10.1007/978-0-387-47946-0>

[22] Jiang, J.: Asymptotic Analysis of Mixed Effects Models: Theory, Applications, and Open Problems. Monographs on Statistics and Applied Probability Series. CRC Press, Boca Raton, Florida (2017). <https://doi.org/10.1201/9781315119281>

[23] Jiang, J., Wand, M. P., Bhaskaran, A.: Usable and Precise Asymptotics for Generalized Linear Mixed Model Analysis and Design. *Journal of the Royal Statistical Society: Series B (Statistical Methodology)* **84**(1), 55-82 (2022). <https://doi.org/10.1111/rssb.12473>

[24] Ma, Y., Jiang, Y., Huang, W.: Tail index varying coefficient model. *Communications in Statistics - Theory and Methods* **48**(2), 235-256 (2019). <https://doi.org/10.1080/03610926.2017.1406519>

[25] Magnus, J. R., Neudecker, H.: Matrix Differential Calculus with Applications in Statistics and Econometrics. John Wiley & Sons, New Jersey (1988).

[26] Miyata, Y.: Fully Exponential Laplace Approximations Using Asymptotic Modes. *Journal of the American Statistical Association* **99**(468), 1037-1049 (2004). <https://doi.org/10.1198/016214504000001673>

[27] Molina, I., Corral, P., Nguyen, M.: Estimation of poverty and inequality in small areas: review and discussion. *TEST* **31**(4), 1143-1166 (2022). <https://doi.org/10.1007/s11749-022-00822-1>

[28] Molina, I., Rao, J.N.K.: Small area estimation of poverty indicators. *The Canadian Journal of Statistics* **38**(3), 369-385 (2010). <https://www.jstor.org/stable/27896031>

[29] Nie, L.: Convergence rate of MLE in generalized linear and non-linear mixed-effects models: Theory and applications. *Journal of Statistical Planning and Inference* **137**(6), 1787-1804 (2007). <https://doi.org/10.1016/j.jspi.2005.06.010>

[30] R Core Team (2021) R: A Language and Environment for Statistical Computing. Vienna, Austria: R Foundation for Statistical Computing. <https://www.R-project.org/>

[31] Rao, J.N.K., Molina, I.: Small Area Estimation. Wiley Series in Survey Methodology. John Wiley & Sons, Hoboken, New Jersey (2015). <https://doi.org/10.1002/9781118735855>

[32] Rohrbeck, C., Tawn, J.: Bayesian Spatial Clustering of Extremal Behavior for Hydrological Variables. *Journal of Computational and Graphical Statistics* **30**(1), 91-105 (2021). <https://doi.org/10.1080/10618600.2020.1777139>

- [33] Ruppert, D., Wand, M. P., Carroll, R. J.: Semiparametric Regression. Cambridge Series in Statistical and Probabilistic Mathematics. Cambridge University Press, New York (2003). <https://doi.org/10.1017/CBO9780511755453>
- [34] Santner, T. J., Duffy, D. E.: The Statistical Analysis of Discrete Data. Springer Texts in Statistics. Springer, New York (1989). <https://doi.org/10.1007/978-1-4612-1017-7>
- [35] Sugashawa, S., Kubokawa, T.: Small area estimation with mixed models: a review. *Japanese Journal of Statistics and Data Science* **3**(2), 693-720 (2020). <https://doi.org/10.1007/s42081-020-00076-x>
- [36] Tierney, L., Kass, R. E., Kadane, J. B.: Fully Exponential Laplace Approximations to Expectations and Variances of Nonpositive Functions. *Journal of the American Statistical Association* **84**(407), 710-716 (1989). <https://doi.org/10.1080/01621459.1989.10478824>
- [37] Torabi, M.: Spatial generalized linear mixed models in small area estimation. *Canadian Journal of Statistics* **47**(3), 426-437 (2019). <https://onlinelibrary.wiley.com/doi/abs/10.1002/cjs.11502>
- [38] Wang, H. J., Li, D.: Estimation of Extreme Conditional Quantiles Through Power Transformation. *Journal of the American Statistical Association* **108**(503), 1062-1074 (2013). <https://doi.org/10.1080/01621459.2013.820134>
- [39] Wang, H. J., Li, D., He, X.: Estimation of High Conditional Quantiles for Heavy-Tailed Distributions. *Journal of the American Statistical Association* **107**(500), 1453-1464 (2012). <https://doi.org/10.1080/01621459.2012.716382>
- [40] Wang, H., Tsai, C. L.: Tail Index Regression. *Journal of the American Statistical Association* **104**(487), 1233-1240 (2009). <https://doi.org/10.1198/jasa.2009.tm08458>
- [41] Weber, M.: A weighted central limit theorem. *Statistics & Probability Letters* **76**(14), 1482-1487 (2006), <https://doi.org/10.1016/j.spl.2006.03.007>
- [42] Wu, L.: Mixed Effects Models for Complex Data. Monographs on Statistics and Applied Probability Series. CRC Press, Boca Raton, Florida (2009). <https://doi.org/10.1201/9781420074086>
- [43] Youngman, B. D.: Generalized Additive Models for Exceedances of High Thresholds With an Application to Return Level Estimation for U.S. Wind Gusts. *Journal of the American Statistical Association* **114**(528), 1865-1879 (2019). <https://doi.org/10.1080/01621459.2018.1529596>
- [44] Youngman, B. D.: evgam: An R Package for Generalized Additive Extreme Value Models. *Journal of Statistical Software* **103**(3), 1-26 (2022). <https://doi.org/10.18637/jss.v103.i03>
- [45] Yoshida, T.: Asymptotic theory for extreme value generalized additive models. arXiv, (2023). <https://doi.org/10.48550/arXiv.2303.02402>